Engineering xxx (xxxx) xxx

Contents lists available at ScienceDirect

Engineering

journal homepage: www.elsevier.com/locate/eng

Research
Large Offshore Floating Structures—Review

Computational Fluid Dynamics Technologies and Applications for Offshore Floating Structures: Progress and Perspectives

Weiwen Zhao [a], Wentao Wang [a,b], Genglu Zhang [c], Decheng Wan [a,*], Frederick Stern [d], Moustafa Abdel-Maksoud [e]

[a] Computational Marine Hydrodynamic Lab (CMHL), School of Naval Architecture, Ocean and Civil Engineering, Shanghai Jiao Tong University, Shanghai 200240, China
[b] China Ship Scientific Research Center, Wuxi 214082, China
[c] Ningbo Pilot Station, Ningbo Dagang Pilotage Co., Ltd., Ningbo 315100, China
[d] IIHR-Hydroscience and Engineering, University of Iowa University, Iowa City, Iowa 52242, USA
[e] Hamburg University of Technology (TUHH), Institute for Fluid Dynamics and Ship Theory (M8), Hamburg 21073, Germany

ARTICLE INFO

Article history:
Received 4 October 2024
Revised 20 July 2025
Accepted 18 November 2025
Available online xxxx

Keywords:
CFD
Marine hydrodynamics
Free-surface flows
Turbulent flows
Complex motion response
Coupling systems

ABSTRACT

Offshore floating structures face intricate multiscale flows, making their design a significant engineering challenge. Computational fluid dynamics (CFD) has become indispensable in designing these structures and their components. Beyond design purposes, CFD deepens fundamental understanding by revealing fluid dynamics in previously poorly characterized flows. This paper reviews current CFD technologies and their applications in offshore floating structures while exploring future prospects. The key challenges are identified to guide professionals in extending technology lifecycles and enhancing capabilities. These insights underscore a crucial research direction for developing the next generation of offshore floating structures.

1. Introduction

With rapid advancements in marine and ocean engineering, an increasing number of offshore floating structures are being deployed and maintained in ocean regions far from the shore. These structures are typically designed on a large scale to meet comprehensive engineering requirements and endure harsh environments. However, the hydrodynamic behavior, structural loads, and dynamic responses of offshore floating structures remain insufficiently understood owing to factors such as wave nonlinearity, fluid viscosity, turbulence, significant motion amplitudes, and coupling among multicomponent systems. Conventionally, the hydrodynamic performance of offshore floating structures has been primarily assessed using potential flow theory, which is effective in most practical engineering design scenarios [1,2]. However, potential flow theory neglects viscous effects, which are essential for accurately determining hydrodynamic performance and structural integrity, particularly in cases involving strong nonlinearities. This limitation becomes particularly apparent under extreme sea conditions, such as wave breaking, turbulent flows, and large-amplitude motions [3,4]. In these scenarios, viscous effects are crucial as they account for the complex fluid–structure interactions, energy dissipation, and vorticity generation essential for understanding system behavior. Offshore floating structures consist of components like floating bodies, mooring lines, flexible risers, and rotors. The dynamic interactions among these components are vital for reliable design and must be considered to ensure the safety of floating structures. Therefore, scientists and engineers are exploring advanced computational methods to more accurately predict overall performance and overcome the limitations of conventional approaches in capturing the intricate physics of offshore floating structures.

In recent decades, research on the theory and application of computational fluid dynamics (CFD) in offshore floating structures has grown rapidly. CFD methods remain a significant area of ongoing research in ocean engineering, as highlighted in a

* Corresponding author.
E-mail address: dcwan@sjtu.edu.cn (D. Wan).

https://doi.org/10.1016/j.eng.2025.11.008

Please cite this article as: W. Zhao, W. Wang, G. Zhang et al., Computational Fluid Dynamics Technologies and Applications for Offshore Floating Structures: Progress and Perspectives, Engineering, https://doi.org/10.1016/j.eng.2025.11.008

review by Tavakoli et al. [5]. According to the International Ship and Offshore Structures Congress (ISSC) Committee I.1: Environment [3], substantial progress has been made in fully nonlinear CFD modeling of waves in recent years, with much emphasis on detailed simulations of steep or breaking wave events, particularly for wave impact applications in offshore structures. The committee emphasized that, despite significant advancements in CFD-based techniques for accurately modeling waves and loading events, these methods remain computationally intensive. While nonlinear potential flow methods offer computational efficiency, they fall short in reliably modeling wave breaking and stability phenomena. Combining viscous CFD with potential flow theory, employing varying levels of accuracy for specific objectives, emerges as a promising approach for long-term wave impact assessments. In structural load and response analyses, CFD methods currently lack the efficiency to address the wide array of wave cases arising from complex environmental conditions across diverse sea states. Nonetheless, they are indispensable for investigating wave loading associated with deterministic wave events and for validating simplified analytical or numerical methods [4]. Additionally, there is increasing demand for comprehensive performance analyses of offshore floating structures in wave conditions, moving beyond isolated studies of phenomena such as rigid body dynamics, slamming, sloshing, and green water effects, which remain critical areas of focus [6]. Numerous literature reviews have explored advancements in CFD applications within ship and ocean engineering [7] and for floating offshore wind turbines (FOWTs) [8]. This review specifically examines CFD modeling techniques and their applications for floating offshore structures, which pose unique challenges due to their dynamic responses, complex environmental interactions, and coupled motions.

Thus, this study offers a thorough review of CFD modeling techniques and their applications in offshore floating platforms. The objective is to outline ① CFD methodologies for simulating intricate environmental flows, encompassing two-phase interfacial and turbulent flows, ② advanced models for nonlinear motion responses and coupled systems, and ③ CFD applications of these techniques in ocean engineering. Computational approaches for two-phase interfacial and turbulent flows are detailed in Sections 2 and 3, respectively. The advanced modeling strategies for nonlinear motion are explored in Section 4. Thereafter, the modeling of complex coupled systems is presented in Section 5, emphasizing comprehensive performance prediction while maintaining computational efficiency and accuracy. The CFD applications for various complex flows and structures related to offshore floating platforms are presented in Section 6. Finally, the future perspectives are discussed in Section 7, with their concluding remarks in Section 8.

2. Two-phase interfacial flow

Two-phase interfacial flows are pivotal in offshore engineering, especially in analyzing localized structural features where precise flow details are crucial for accurate performance forecasts. These flows, involving interactions between immiscible fluids like water and air, are essential for comprehending phenomena such as wave impact, slamming, sloshing, and green water loading on floating offshore structures. Precisely capturing two-phase interfacial flow details is critical, as even slight inaccuracies can result in substantial errors in predicting structural loads, dynamic responses, and overall system behavior. Advanced interface-capturing techniques, including volume of fluid (VOF) and level-set methods, have been developed to model complex flows with high fidelity [9].

2.1. Volume of fluid

The VOF method is widely employed for modeling two-phase interfacial flows due to its maturity, robustness, and inherent mass-conservation properties. It utilizes a scalar function, known as the volume fraction, which ranges from 0 to 1 to differentiate between two immiscible fluids. The volume fraction represents the ratio of the tracked fluid volume to the cell volume. The governing equation for the advection of the volume fraction is

$$\frac{\partial \alpha}{\partial t} + \nabla \cdot (\boldsymbol{u}\alpha) = 0 \tag{1}$$

where α denotes the volume fraction, t is the time, ∇ represents the divergence, and $\boldsymbol{u}$ is the velocity field. Here, $\alpha = 0$ and $\alpha = 1$ signify that the cell is entirely filled with water and air, respectively, while $0 < \alpha < 1$ denotes the interface between the two fluids. Once α is determined for each grid cell, the interface is consequently constructed.

The volume fraction serves as a discontinuous field function across cells at the interface. Solving Eq. (1) directly without specialized treatment for the convection term introduces excessive diffusive errors, hindering the ability to achieve a smooth volume fraction field near the interface. To maintain a sharp interface, specific schemes and algorithms must be implemented to solve Eq. (1). Based on the solutions to Eq. (1) and the advection of the volume fraction, VOF methods are generally classified into algebraic and geometric VOF methods.

Algebraic VOF methods perform algebraic calculations to determine the flux of volume fractions and execute advective operations based on the computed flux. Eq. (1) is typically solved directly using partial differential equations (PDEs) with high-order nonoscillatory advection schemes for interface antidiffusion. One such method involves interface compression techniques that employ specialized high-resolution schemes. Examples include the compressive interface capturing scheme for arbitrary meshes (CICSAM) [10], high-resolution interface capturing (HRIC) scheme [11], switching technique for advection and capturing of surfaces (STACS) [12], higher-resolution artificial compressive (HiRAC) formulation [13], and modified CICSAM (M-CICSAM) [14], many of which are commonly used in commercial CFD codes. Among open-source CFD codes, OpenFOAM (OpenFOAM Foundation, UK) utilizes the widely adopted algebraic VOF approach. This method incorporates an interface compression term into the volume-fraction equation and solves it using the multidimensional universal limiter with explicit solution (MULES) scheme [15]. Owing to the avoidance of complex geometric operations and its straightforward implementation on unstructured grids [16], algebraic VOF methods are available in both commercial and open-source CFD codes and have been extensively used for industrial flow simulations. However, algebraic operations can disrupt the discontinuous nature of the volume-fraction field, potentially introducing interpolation and discretization errors. Larsen et al. [16] evaluated the performance of a VOF implementation in OpenFOAM for a wave-propagation problem under periodic boundary conditions. Their results showed that prolonged numerical simulations led to nonphysical oscillations in the wave crests, caused by the numerical dispersion and diffusion inherent to algebraic VOF schemes. An alternative approach to interface antidiffusion is the tangent of a hyperbola for interface capturing (THINC) [17]. The THINC scheme computes flux through cell faces by approximating the volume fraction field using a hyperbolic tangent function. Comparative studies [18,19] have demonstrated that THINC-based schemes achieve accuracy comparable to geometric VOF methods without incurring additional computational costs. However, the performance of algebraic VOF methods necessitates thorough evaluation through extensive, realistic simulations.

In contrast to algebraic VOF methods, geometric VOF approaches explicitly reconstruct interfaces via geometric computations [20]. Initially, these methods were largely confined to structured grids due to algorithmic complexity and implementation challenges [21,22]. Recently, significant research efforts have focused on enhancing geometric VOF methods for unstructured grid applications. Roenby et al. [23] developed isoAdvector, an innovative geometric VOF method tailored for arbitrary polyhedral unstructured grids in OpenFOAM. This approach constructs an approximate interface by connecting volume fraction isopoints along grid cell edges to form an isosurface. The reconstructed interface was not limited to a planar configuration, potentially resulting in surface warping. Comparative studies have shown that isoAdvector outperforms the native interface-compression algebraic VOF methods of OpenFOAM in practical ocean engineering applications, particularly hydrodynamic problems. Larsen et al. [16] demonstrated that isoAdvector effectively eliminates numerical artifacts, especially free-surface wrinkles, in wave propagation simulations across grids with varying aspect ratios, thereby producing significantly smoother wave surfaces.

Building upon prior research, Scheufler and Roenby [24] developed an advanced iterative interface reconstruction scheme (isoAdvector-plicRDF) that integrates a reconstructed distance function following the framework of Cummins et al. [25]. This enhanced approach significantly reduces reconstruction errors and improves computational efficiency. However, recent studies reveal that isoAdvector–plicRDF may forfeit second-order accuracy when the Courant number exceeds 0.2 [26]. Utilizing the isoAdvector methodology, the authors also introduced TwoPhaseFlow, an open-source library for two-phase flow simulations [27]. Progressing geometric VOF methods, Dai and Tong [28] devised analytical interface reconstruction algorithms for piecewise linear interface calculation (PLIC) within arbitrary convex polyhedral cells, achieving lower truncation errors and decreased computational complexity. Simultaneously, López and Hernández [29] created gVOF, a comprehensive software package that implements multiple geometric VOF methods for various mesh types, including structured and unstructured grids with both convex and non-convex cells. Anchored in multidimensional unsplit advection and PLIC schemes, gVOF aims to facilitate the broader adoption of accurate and computationally efficient geometric unsplit VOF methods in CFD applications.

The VOF method inherently ensures mass conservation, making it highly suitable for simulations requiring precise volume preservation. Its proficiency in modeling complex interfacial phenomena—such as wave breaking, droplet splashing, and air entrainment—has established it as an industry standard in both commercial and open-source CFD software. This widespread acceptance is attributed to the optimal balance of the method between computational efficiency and physical fidelity. Nevertheless, the VOF approach inherently struggles to maintain sharp interfaces due to numerical diffusion. While geometric VOF reconstruction techniques can reduce interfacial smearing by offering a more accurate surface representation, their complex implementation often undermines computational robustness and parallel scalability, particularly in turbulent free-surface flows with complex geometries.

2.2. Level-set

Level-set methods, initially developed by Osher and Sethian [30] and Sethian and Smereka [31], represent the interface $\Gamma(t)$ as the zero level set of a continuous signed-distance function (SDF; $\varphi(\boldsymbol{x},t)$), written as $\Gamma(t)=\{\boldsymbol{x}\in\Omega_1+\Omega_2;\quad \varphi(\boldsymbol{x},t)=0\}$ (where $\boldsymbol{x}$ is the coordinates, Ω_1 and Ω_2 are two fluid regions). These methods solve the level-set transport equation.

$$\frac{\partial\varphi}{\partial t}+\nabla(\boldsymbol{u}\cdot\varphi)=0 \tag{2}$$

Typically, the equation is discretized using a weighted essentially non-oscillatory (WENO) scheme for spatial discretization and a high-order total variation diminishing Runge–Kutta scheme for temporal integration.

The initial value of $\varphi(\boldsymbol{x},t)$ is defined as follows:

$$\varphi(\boldsymbol{x},0)=\begin{cases}\text{dist}(\boldsymbol{x},\Gamma(0)) & \boldsymbol{x}\in\Omega_1\\ 0 & \boldsymbol{x}\in\Gamma(0)\\ -\text{dist}(\boldsymbol{x},\Gamma(0)) & \boldsymbol{x}\in\Omega_2\end{cases} \tag{3}$$

Since the field is a continuous function, level-set methods not only maintain a sharp interface but also accurately compute interface curvature and surface tension. However, a fundamental limitation exists: The SDF loses its signed-distance property during advection, necessitating re-initialization at each time step. This characteristic leads to poor mass conservation, significantly hindering full resolution efforts. Recently, various mitigation strategies have been introduced, including subcell corrections [32], hybrid particle level-set methods [33], high-resolution mesh refinements [34], and adaptive mesh refinement (AMR) [35]. Although these improvements have partially resolved mass conservation issues, they inevitably add computational complexity, thereby reducing the original simplicity and diminishing the appeal of the level-set method.

An alternative approach to address mass conservation issues utilizes conservative level-set methods, wherein the signed distance function is replaced by a smooth Heaviside function, representing interfaces through diffuse profiles [36,37]. In this framework, the interface is advected by numerically solving a reinitialization equation for the Heaviside function. Total variation diminishing (TVD) schemes are typically employed for advection to ensure solution robustness while minimizing dispersion errors. Although numerous enhancements to conservative level-set methods have been proposed [38–40], a comprehensive discussion of these developments lies beyond the scope of this review.

The level-set method offers a distinct and continuous representation of the interface, making it highly effective for precise curvature calculations and surface-tension modeling. This capability renders it particularly suitable for high-fidelity simulations of interfacial phenomena, including bubble dynamics and droplet interactions. Its implicit representation inherently manages topological changes such as the merging or splitting of interfaces. However, the method possesses inherent nonconservative properties, potentially resulting in significant mass errors in extensive or large-domain simulations. Additionally, periodic reinitialization is required to maintain the signed distance property of the level-set function, leading to increased computational costs. These attributes make the level-set approach ideal for applications necessitating accurate interface tracking, such as wave slamming, green water loading, and other impact-related phenomena, though it may be less suitable for mass-sensitive applications.

2.3. Coupled level-set VOF

To integrate the strengths of the level-set and VOF methods, Sussman and Puckett [41] introduced the coupled level-set and VOF (CLSVOF) method. The CLSVOF method ensures effective mass conservation while maintaining a sharp interface. Moreover, it provides precise geometric details of the interface, including normal vectors and curvatures. CLSVOF methods are categorized into one-way and two-way coupling based on their coupling strategies.

In the one-way coupling approach, the level-set function is not directly solved but is derived from the volume fraction. Kunkelmann and Stephan [42] did not explicitly solve the transport

equation for the level-set function at each timestep; instead, they estimated the level-set field by updating the volume-fraction field to reconstruct the interface. Similarly, Albadawi et al. [43] developed the simple coupled level-set and volume of fluid (S-CLSVOF) method, which emphasizes improved surface tension calculations. Comparisons with the interface compression algebraic VOF method showed that the S-CLSVOF method significantly enhances the accuracy of bubble dynamics problems dominated by surface tension.

In the two-way coupling approach, both the level-set function and volume fraction are updated by solving their respective transport equations with mutual corrections. Wang et al. [44] implemented the CLSVOF method within their in-house Cartesian grid solver, CFDShip-Iowa v6. Dianat et al. [45] applied the CLSVOF method in OpenFOAM on arbitrary polyhedral unstructured grids using an enhanced clipping-and-capping algorithm proposed by Skarysz et al. [46] for PLIC-based interface reconstruction and a gradient calculation method tailored for unstructured grids during the reinitialization of the level-set function. Zhao and Chen [47] implemented the CLSVOF method in an overset grid system.

Although CLSVOF methods offer superior accuracy compared to standalone level-set or VOF approaches, they entail substantially higher computational costs due to their complexity. The parallel scalability of the method is particularly challenging, as it requires the synchronized execution of both level-set and VOF computations. Additionally, CLSVOF is susceptible to numerical diffusion in regions with intricate interface dynamics and demands meticulous parameter tuning for optimal performance. These limitations highlight the necessity for continued development to improve the suitability of CLSVOF for large-scale ocean engineering simulations, especially in enhancing computational efficiency and parallel implementation.

2.4. Ghost fluid method

Several studies on VOF-based two-phase flow simulations have reported spurious air velocities above free surfaces (FSs) [48]. This numerical artifact stems from the conventional VOF method's handling of interfacial properties, where flow variables are calculated as weighted averages of both phases. Such averaging inadequately enforces jump conditions at the interface, particularly in flows with large density ratios between phases, leading to unphysical velocity fields. To address this, the ghost fluid method (GFM) was developed to eliminate spurious air velocities in two-phase interfacial flow simulations. As illustrated in Fig. 1, p_d is the dynamic pressure and x is the coordinate. P, N, and f denote field values at two adjacent cell centers and their shared face center, respectively. Γ_f represents the free surface interface. The linear interpolation scheme calculates the face-center value p_{df} without considering the pressure jump across the interface Γ_f, which results in an incorrect and unphysical pressure gradient. GFM constructs ghost cells across the interface and populates them with appropriately extrapolated quantities denoted by superscripts "+" and "−" for the opposing phase. By meticulously maintaining discretized interface jump conditions, GFM effectively segregates the two-phase problem into distinct single-phase flow domains, enforcing interfacial conditions via ghost cell values.

Initially introduced by Fedkiw et al. [49] for compressible two-phase flows alongside the level-set method on a finite difference Cartesian grid solver, GFM was subsequently extended to incompressible air–water flows [50]. Huang et al. [51] developed an integrated ghost fluid and two-phase level-set method, formulating approximate jump conditions for piezometric pressure, velocity, and pressure gradients. Validated using flow around the DTMB 5512 hull, the method exhibited exceptional performance and demonstrated substantial potential for managing complex turbulent flows in ship hydrodynamics. Yang and Stern [52] combined the level set/GFM with large-eddy simulation (LES) and an immersed boundary (IB) approach for moving bodies. Wang and Stern [53] employed a hybrid ghost fluid and geometric VOF method, introducing a ghost fluid cell interpolation formula that eliminates the need to determine the precise FS position. Vukčević et al. [54] were the first to implement GFM within the arbitrary polyhedral framework of OpenFOAM for large-scale air–water flows. Surface tension was neglected, and viscosity was assumed to be continuous across the interface. Building on Vukčević's work, Peltonen et al. [55,56] introduced jump conditions for both pressure and viscosity, highlighting the importance of accurately handling the viscosity term through a two-dimensional (2D) shear layer test case. Kanninen et al. [57] improved interface location by developing a new formulation for weighting parameters, thereby addressing the insufficient propagation of small-amplitude waves. Chen et al. [58] implemented the GFM in OpenFOAM and applied it to wave–structure interaction problems using a modified generating–absorbing boundary condition.

The GFM achieves enhanced interface sharpness without incurring numerical diffusion, demonstrating its efficacy in handling significant discontinuities at air–water interfaces with high density ratios. This technique accurately enforces jump conditions for pressure, density, and other physical quantities across the interface, making it theoretically well-suited for multiphase flow simulations. However, implementing GFM requires sophisticated interface reconstruction algorithms and specialized boundary condition treatments, considerably increasing computational complexity. Despite its potential, GFM remains underutilized in free-surface flow applications compared to established methods like VOF or level-set approaches. Additional validation studies are necessary to assess its performance in complex offshore engineering scenarios, such as wave–structure interactions, breaking waves, and other intense free-surface phenomena.

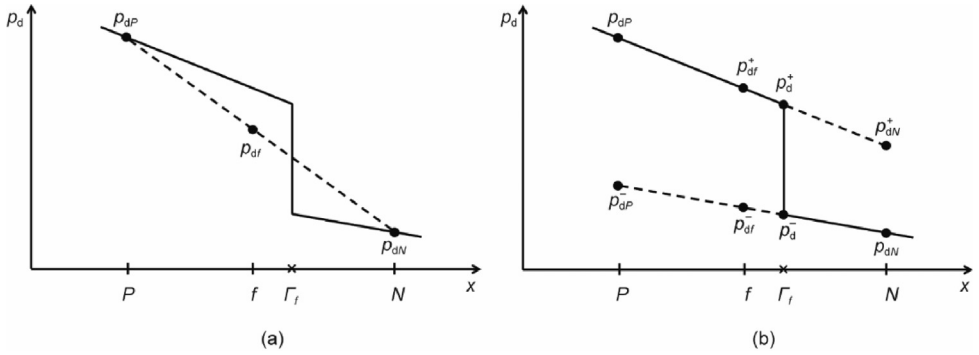

Fig. 1. Cell-face interpolation scheme of the interfacial cells. (a) Linear interpolation scheme; (b) interpolation scheme considering FS jump conditions

3. Turbulent and wake flows

Offshore floating structures encounter a wide array of complex turbulent and wake flows due to dynamic oceanic conditions. These flows include turbulence induced by breaking waves, wake flows around column structures, and wake effects behind wind turbines. Accurately representing such flows requires the careful selection of suitable turbulence models, as different regions around offshore structures may exhibit distinct turbulent characteristics. For wave loads involving non-breaking waves, turbulence effects can often be neglected without significantly compromising prediction accuracy. However, in the case of large-amplitude waves with breaking phenomena, turbulence is crucial for accurately modeling FS evolution, energy dissipation, and flow dynamics during breaking events. Furthermore, turbulence cannot be ignored when simulating wind and current loads, as it profoundly influences fluid forces and structural responses.

3.1. Breaking wave-induced turbulence

Wave-induced turbulence in ocean engineering encompasses both wave propagation and breaking phenomena. Conventional Reynolds-averaged Navier–Stokes (RANS) methods tend to generate excessive eddy viscosity near the FS, resulting in substantial numerical damping of FS flows (Fig. 2 [59]). To mitigate this issue, Devolder et al. [60] introduced an enhanced model that markedly improves the accuracy of simulating wave breaking by integrating buoyancy-modified k–ω and k–ω shear stress transport (SST) turbulence models (where k is the turbulent kinetic energy and ω is the specific dissipation rate). Evaluated within the OpenFOAM framework, these models accurately predicted surface elevations, undertow profiles, and turbulent kinetic energy levels, particularly for spilling and plunging breakers. The inclusion of a buoyancy term corrected the overestimation of turbulence kinetic energy, providing a more precise representation of the flow field. The study concluded that the buoyancy-modified k–ω model outperforms other models in simulating wave breaking. Additionally, Larsen and Fuhrman [61] addressed the persistent problem of significantly overestimated turbulence levels in RANS models by developing a novel k–ω turbulence closure model. This model effectively stabilizes nearly potential flow regions, resolving the unconditional instability that has afflicted existing two-equation turbulence models. Demonstrating superior performance, the new model accurately simulated both non-breaking and breaking waves, capturing pre- and post-breaking surface elevations, turbulence profiles, and undertow velocities without the exponential growth of eddy viscosity that plagued previous studies. This advancement is crucial for enhancing the accuracy of CFD simulations in coastal and maritime engineering applications.

3.2. Wake flows in current

Offshore floating platforms generally comprise simple geometric forms, such as cylinders, cubes, and other regular shapes, assembled in various configurations. Precise forecasting of current loads necessitates accurate modeling of flow separation and wake dynamics, which are pivotal for comprehending the hydrodynamic forces acting upon these structures. Such precision is crucial for predicting dynamic behaviors like vortex-induced vibrations (VIV) or vortex-induced motions (VIM), which can markedly impact platform stability and fatigue lifespan. Advanced CFD methodologies, including turbulence modeling and high-resolution simulations, are essential for capturing these intricate flow phenomena and ensuring dependable structural performance evaluations.

For long, slender, and flexible risers, accurately modeling wake flows is vital for forecasting the VIV response. To mitigate computational expenses, the 2D strip method introduced by Willden and Graham [62,63] is extensively utilized. In the 2D strip approach, the fluid flow is treated as locally 2D without spanwise correlation, thus simplifying the three-dimensional (3D) fluid field into multiple 2D strips uniformly distributed along the span of the cylinder. Within each 2D strip, the fluid flow is typically resolved using the RANS method [64]. Duanmu et al. [65] developed the viv-FOAM-SJTU solver and performed numerical simulations of VIV in a vertical riser subjected to stepped currents. Fu and Wan [66] and Fu and Zou [67] employed viv-FOAM-SJTU to simulate VIV responses of a flexible riser in oscillatory flows, revealing that the oscillating riser interacts with wake flows. This interaction induces significant 3D characteristics in the flow, which cannot be captured by the 2D strip method. Deng et al. [68] developed viv3D-FOAM-SJTU, a 3D thick strip solver, to predict the VIV response of flexible cylinders. Utilizing the RANS method with the SST k–ω turbulence model, the solver efficiently captures the complex hydrodynamic forces within each fluid strip.

The 3D strip model significantly enhances prediction accuracy by incorporating axial flow field correlations, which are crucial for depicting the 3D aspects of vortex shedding, as displayed in Fig. 3 [68]. The validity of the solver was established through extensive comparisons with experimental data and published numerical simulations, proving its effectiveness in forecasting VIV amplitudes, modes, and frequencies. Subsequently, Hu et al. [69] integrated the SST-delayed detached eddy simulation (SST-DDES) method into the viv3D-FOAM-SJTU solver to include axial flow correlations in 3D wake flows. They applied this improved solver to examine the VIM response of slender flexible risers with grooved and spanwise strips, thereby demonstrating its ability to capture intricate 3D flow interactions and their effects on structural dynamics.

Similar to VIV, column-stabilized floating offshore structures undergo VIM due to periodic vortex shedding around their columns. Accurate prediction of flow separation and wake dynamics is essential for assessing the VIM response. In VIM, wake flows exhibit pronounced three-dimensionality due to the complex geometries of floating platforms, such as helical strakes on spars, pontoons on semi-submersibles, and free ends at the column bases. Yin et al. [70] identify RANS, detached-eddy simulation (DES), and LES as the primary turbulence modeling methods for VIM predictions. DES, a hybrid approach combining RANS and LES, is increasingly preferred for VIM analysis due to its ability to

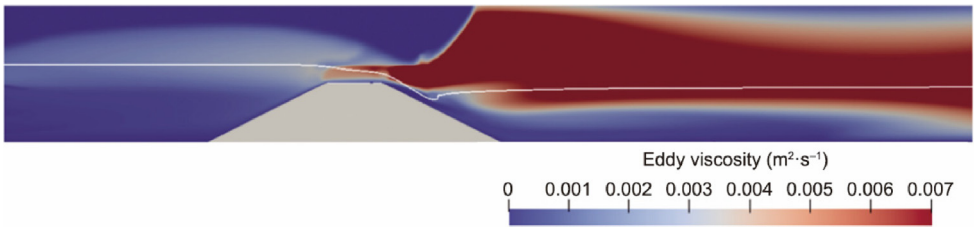

Fig. 2. Eddy-viscosity contours for plunging jet flow on a hump [59].

Fig. 3. Vortex shedding of a flexible riser predicted by 2D and 3D strip theory. Reproduced from Ref. [68] with permission of Elsevier, ©2020.

accurately predict highly unsteady and separated flows while requiring less mesh refinement than LES. DES methodologies have demonstrated significant advantages in forecasting local, separated, and wake flows, particularly when flow separation is expected [71]. Kim et al. [72] investigated the impact of VIM on offshore floating structures, including oil and wind turbine platforms, using both a delayed detached eddy simulation (DDES) turbulence model and an unsteady RANS (URANS) model to evaluate and optimize their designs. They conducted a CFD sensitivity analysis, examining the effects of turbulence models, mesh refinement, and time step selection on simulation results, and validated the CFD findings with towing tank experiments. The study found that the DDES turbulence model was more accurate than the URANS model in predicting VIM, particularly in capturing vortex structures.

Kara et al. [73] utilized the open-source CFD software OpenFOAM to simulate and assess the VIM response of floating structures, such as semi-submersible platforms. They validated the CFD approach by comparing it with model test data. The study also indicates that the DES turbulence model effectively estimates response amplitudes and periods, recommending it for CFD-based VIM simulations. Chen and Chen [74] performed numerical simulations of the VIM response of a semi-submersible using the finite-analytic Navier–Stokes (FANS) code combined with the LES method and a moving overset grid approach. They utilized DES calculations to validate the LES model.

3.3. Wake flows in wind

Wake flows behind wind turbines significantly influence energy extraction and the turbulence intensity of downstream turbines. To simulate these wake flows, RANS and LES are typically employed alongside the actuator line model (ALM), initially developed by Sørensen and Shen [75]. The ALM method used a set of discretized actuator points to represent the blades. Section lift and drag forces are computed by the local flow velocity and angle of attack, which will be determined from an airfoil lookup table, as show in Fig. 4. Bachant et al. [76] conducted a comprehensive study on the development and validation of an ALM for vertical-axis turbines, integrated with k–ε RANS. The ALM, which blends classical blade element theory with Navier–Stokes flow models, has been effectively applied to high- and medium-solidity vertical-axis turbines, demonstrating a substantial reduction in computational cost compared to 3D blade-resolved RANS simulations. They found that ALM, when coupled with RANS, provides a cost-effective and reasonably accurate tool for predicting turbine performance and wake dynamics, making it invaluable for engineering and research in wind and marine hydrokinetic turbines. Despite some discrepancies in turbulence predictions, ALM offers a more physical flow description and bridges the gap between low- and high-fidelity flow modeling, warranting further development and refinement for future applications. Stevens et al. [77] developed an LES solver integrated with ALM and the actuator disk model (ADM). Wind farm simulation results were benchmarked against wind turbine measurements, demonstrating that the ALM method more effectively captured wake dynamics.

4. Complex motion response

Offshore floating structures exhibit intricate six-degree-of-freedom (6DOF) motion responses when subjected to environmental forces such as waves, wind, and currents. Precise modeling of these 6DOF motions is essential for evaluating structural integrity, stability, and operational safety. However, numerically simulating these dynamics is challenging due to factors like large-amplitude motions, added-mass instability, and mesh movement.

4.1. Six-degree-of-freedom motion and added-mass instability

Typically, two coordinate systems are employed to describe the 6DOF motions of floating structures: a local non-inertial coordinate system and a global inertial coordinate system [78,79]. The local coordinate system is fixed to the structure, moving and rotating with the body, which simplifies the representation of the forces and moments acting on the structure. In contrast, the global coordinate system serves as a stationary reference frame to monitor the absolute position and orientation of the floating body in space. These coordinate systems coincide only when the structure maintains an even keel. Transformations between them are crucial for accurately resolving forces and moments within CFD solvers. The primary methods for these transformations are the Euler-angle-based approach and the quaternion-based approach.

Euler angles decompose rotations into three sequential steps around the body axes. Despite the issue of gimbal lock, Euler angles remain widely adopted in ocean engineering due to their intuitive alignment with conventional motion descriptors [80]. The quaternion-based method employs quaternions to represent rotations as four-dimensional extensions of complex numbers, thereby preventing gimbal lock by eliminating sequential rotations. This computationally stable approach is favored in modern CFD tools like OpenFOAM, which utilizes a symplectic integration scheme inspired by molecular dynamics [81].

A major challenge in CFD simulations coupled with 6DOF stems from the added-mass effect, where accelerating a rigid body necessitates accelerating the surrounding fluid. This introduces an "artificial" mass proportional to the displaced fluid volume, altering the effective inertia of the system. For low-mass-ratio structures (e.g., tension-leg platforms and buoys), where structural mass is comparable to displaced fluid mass, this effect can destabilize simulations, causing non-physical oscillations in forces, velocities, and displacement.

The added mass instability arises from the explicit coupling of fluid and rigid body motion solvers. In conventional partitioned approaches, fluid forces and structural motions are solved sequentially, creating a time lag that magnifies errors in force predictions. This problem is exacerbated by the Courant–Friedrichs–Lewy (CFL) condition, which restricts time-step sizes in explicit schemes, further increasing computational costs. Dunbar et al. [82] developed a tightly coupled CFD/6DOF solver employing a subiteration loop and dynamic relaxation techniques to eliminate artificial added mass instability. The proposed method is shown to be insensitive to time steps and capable of preventing spurious non-physical oscillations in velocity and force. Chow and Ng [83] enhanced the stability of the OpenFOAM VOF-based solver by implementing a dynamic relaxation scheme. This method iteratively adjusted the pressure field and velocity corrections to account for added mass effects, thereby significantly improving the convergence of low-mass-ratio structures. Bruinsma et al. [84] sought to mitigate added-mass instabilities by applying a pressure field under-relaxation technique alongside a predictor–corrector method. Despite these measures, numerical oscillations due to added mass effects persisted. Stability can be further enhanced using implicit

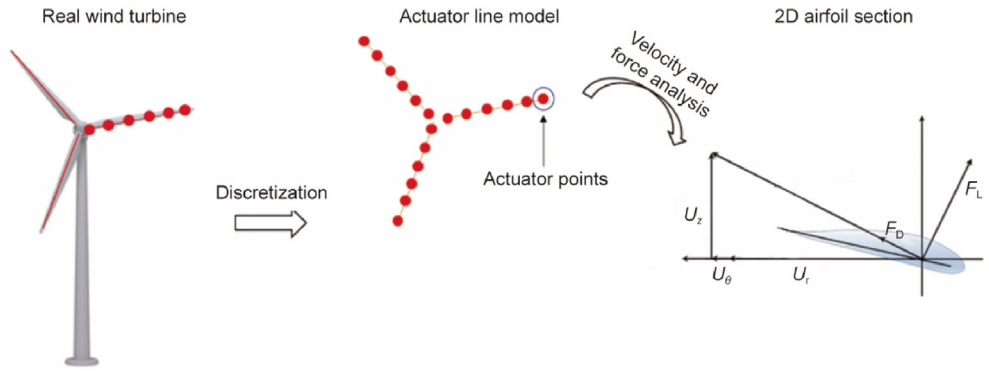

Fig. 4. Discretization of the wind turbine blades in ALM. U_z and U_θ are axial velocity and tangential velocity, respectively. U_r is the linear velocity induced by rotation. F_L and F_D are lift and drag forces on the blade section, respectively.

techniques; however, this typically requires multiple subiterations per time step to achieve convergence between the fluid and motion solvers, leading to a substantial increase in computational time. Devolder et al. [85] introduced an improved coupling algorithm that accelerated convergence by computing a Jacobian matrix from solutions obtained in prior subiterations, thereby reducing computational costs.

Although iterative methods yield accurate results upon convergence, they may lack robustness in certain extreme scenarios. To address these limitations, an alternative approach involves the explicit calculation of added mass. Roenby et al. [86] proposed the floatStepper algorithm to resolve added-mass instability issues. The core algorithm determines the fluid response before each computational time step through a series of prescribed probe body motions, thereby decomposing the net force and torque into two components: ① the added mass contribution proportional to instantaneous body acceleration and ② all other forces and torques. This method allows for the direct and accurate calculation of true body acceleration without requiring external iterations.

4.2. Mesh motion techniques

Mesh motion techniques are classified based on whether the body is rigid or flexible. For rigid-body motion, two principal strategies are commonly employed: dynamic morphing/deforming, which modifies the mesh to accommodate movement, and dynamic overset, which uses overlapping grids to manage complex displacements.

Dynamic morphing mesh techniques enable the simulation of moving boundaries by temporally adjusting the mesh without altering its topology, maintaining element connectivity, and avoiding the computational costs associated with remeshing [87]. This method is particularly effective for small-amplitude body motions, as large displacements can compromise mesh quality through excessive stretching or skewing, leading to numerical inaccuracies [88]. Mesh deformation is governed by three main methods: PDE-based, physical analogy, and interpolation-based techniques. PDE-based methods solve motion equations (e.g., Laplacian or pseudo-solid equations) to propagate boundary displacements to internal nodes [89]. Although they are computationally intensive for large or unsteady meshes, they ensure that interior nodes stay within boundaries, making them robust for both structured and unstructured grids. Physical analogy methods simulate mesh deformation using mechanical analogies, such as spring and elasticity models. The spring analogy treats edges as springs, where boundary displacements induce forces that propagate through the grid [90]. Elasticity methods solve elasticity equations for nodal displacements but necessitate careful calibration of material properties [91,92]. Interpolation methods directly map boundary displacements to interior nodes, utilizing techniques like inverse distance weighting, Delaunay interpolation, and radial basis function (RBF) interpolation [93–96]. Delaunay interpolation utilizes a background grid to transfer boundary motion, making it adaptable to diverse topologies and 3D configurations. RBF interpolation, leveraging smooth algebraic functions, offers significant advantages by operating independently of mesh connectivity and providing deterministic results throughout deformation cycles. These approaches are computationally efficient and aptly suited for handling large or complex deformations; nevertheless, they may require precomputing basis functions to achieve optimal performance.

A dynamic overset mesh can be employed to avert mesh distortion during large-amplitude motion. The adverse effects of body motion on grid quality are alleviated by linking the separated grid segments through interpolation. The overset grid technique involves creating individual meshes for each moving object. Computational meshes may consist of structured or unstructured grids, with overlapping regions among nested grids. During computations, domain connectivity information (DCI) between overlapping grids must be determined. The DCI includes information about the types of grid cells in different regions, as well as the grids and corresponding interpolation weights required for boundary grid interpolation. Fig. 5 [97] depicts a typical arrangement of overlapping grids for a FOWT with rotating blades. Multiple grid sets exchange flow field information via fringe cells, with active cells participating in the flow field solution. Active cells adjacent to fringe cells act as donor cells, providing interpolation data for the fringe cells.

The accuracy and reliability of the overset method critically rely on the conservation properties of overset grids. Chandar [98] demonstrated that nonconservative interpolation methods induce unphysical oscillations or slight deviations from single-mesh results in single-phase flows. Conversely, in two-phase flows with substantial density disparities, such as air and water, interpolation effects become pronounced, leading to the gradual elimination of one phase over time. Teschner & Mundt [99] also noted that employing interpolation techniques to exchange flow variables fails to guarantee their conservation. Chandar's analysis [98] attributes the nonconservative behavior of overset grids to the source term, which preserves the original Poisson equation's form but is defined within overlapping regions. As boundary values are interpolated from adjacent meshes, these source terms become inconsistent throughout the computational domain. This interpolation process inherently undermines solution accuracy, and when the solution representation on overset meshes becomes insufficient,

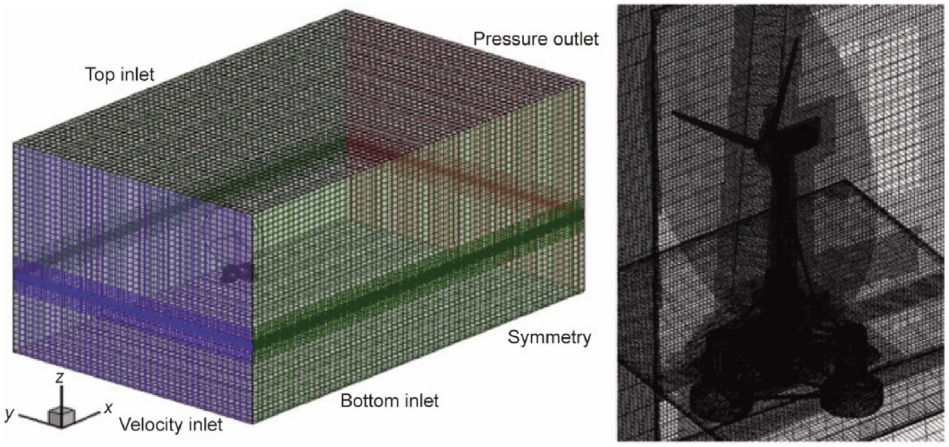

Fig. 5. Dynamic overset grid system of FOWT. Reproduced from Ref. [97] with permission of Elsevier, ©2016.

it results in global mass imbalances and conservation errors. These nonconservation effects appear as pressure oscillations, mass discrepancies, and inaccuracies in interface capture.

Various strategies have been developed to improve overset grid conservation, including local mesh refinement to minimize discretization errors, RBF interpolation for enhanced solution transfer [100], and supermesh techniques to ensure conservative interpolation [101]. Ensuring proper conservation in overset meshes guarantees the accurate preservation of flow variables, thereby enhancing both solution accuracy and numerical convergence.

4.3. Immersed boundary method with adaptive mesh refinement

The IB method is a robust technique for handling complex geometric boundaries and body motions in fluid dynamics. Its core concept entails representing the boundary conditions of intricate geometries as volumetric force sources within the Navier–Stokes equations. Employing simple rectangular grid systems, this approach alleviates the challenges associated with generating body-fitted grids, thereby simplifying mesh generation and facilitating the management of moving boundaries during complex motion responses [102–104].

IB methods are primarily classified into two types based on their treatment of volumetric force sources: continuous and discrete forcing approaches. The continuous forcing approach was initially used for elastic boundary problems, where the volumetric force source expression is based on the material properties of the boundary and directly derived from mechanical relationships. This method was first introduced by Peskin [105] and subsequently enhanced by Goldstein et al. [106] and Saiki and Biringen [107]. These researchers employed feedback forces to represent solid boundaries and imposed no-slip conditions by setting fluid velocity to zero at specific points within the flow field. In contrast, the discrete forcing approach calculates force sources from discretized control equations that often lack analytical expressions. This method is mainly applied to solid-interface problems and includes techniques such as direct forcing [108], cut-cell [109], and ghost-cell methods [110].

Owing to its use of rectangular grid systems, the IB method is typically combined with AMR techniques. Integrating an IB method with a block-structured Cartesian mesh and AMR enables more efficient mesh refinement exclusively in regions determined by flow characteristics [111]. AMR employs a hierarchy of nested rectangular grids, dynamically modifying grid topology during the discretization and solution of control equations. This approach refines grids locally based on flow dynamics and computational demands, thereby enhancing computational efficiency while preserving high local grid resolution. Three primary AMR strategies are commonly utilized: mesh point-based refinement, mesh block-based refinement, and mesh patch-based refinement, as illustrated in Fig. 6.

Adaptive refinement utilizing grid points [112–114] treats grid points as the fundamental elements within a tree structure, where each grid point is subject to partitioning. In contrast, adaptive refinement based on grid blocks [115,116] uses grid blocks as the primary units within the tree structure. Initially, the entire computational domain is divided into one or more grid blocks, each containing a fixed number of grids in every direction. Each grid block can be solved independently. Upon refinement, a grid block is subdivided into four or eight sub-grid blocks. These sub-grid blocks retain the same number of grids as their parent blocks, but their grid sizes are halved relative to the parent block. Adaptive refinement employing grid patches [117] utilizes grid patches as the units within a tree structure. This method does not require parent and sub-grid patches to cover identical spatial ranges nor mandate that each grid patch contains an equal number of grid points. This approach combines the advantages of the two preceding methods: each grid within the computational domain is individually examined and processed, resulting in high refinement efficiency. However, the variable coverage range of the grid patches increases algorithmic complexity. Furthermore, the data structure required for interpolating template points surrounding the grid is complex, and frequent communication can impede program parallelization and pose challenges for load balancing.

5. Coupling systems

5.1. Mooring system-floating body coupling

Accurately evaluating the dynamic performance of moored floating offshore structures necessitates a thorough comprehension of floating-structure hydrodynamics, mooring system dynamics, and their interactions [118]. Various analytical methods,

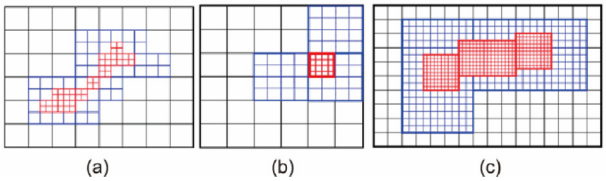

Fig. 6. Adaptive mesh refinement methods based on (a) mesh points, (b) mesh blocks, and (c) mesh patches.

typically categorized as static, quasistatic, or dynamic, have been developed for such systems. Static analysis is frequently utilized in the preliminary design of mooring systems for floating structures, as it effectively establishes the equilibrium position of the system [119]. The quasistatic approach presumes that the oscillations of the moored floating body have small amplitudes and are linear. It neglects drag and inertia effects, assuming constant loads on the mooring lines during each time step. Consequently, the quasistatic method consistently underestimates mooring line tension under extreme conditions. The dynamic method is favored for large-amplitude, low-frequency motions, where the moored floating objects exhibit significant offsets.

Numerous studies have investigated coupled mooring systems and floating bodies. Quallen and Xing [120] integrated a mooring force model with high-resolution CFD using the CFD solver CFDShip-Iowa v4.5. In their model, the mooring lines were represented as catenaries, ignoring stiffness, hydrodynamic forces, and inertial forces. Gutiérrez-Romero et al. [121] compared linear, quasistatic, and dynamic mooring models to assess the dynamic responses of moored floating structures. Their results indicated substantial differences among the mooring models, with the quasistatic model tending to overestimate the mooring lines' fatigue life. Nevertheless, these studies employed potential flow methods that neglected both nonlinearities and viscous effects. Such approaches inadequately predict the oscillatory behavior of floating structures, especially at their natural frequencies, because viscous effects must be simplified, leading to less reliable outcomes under dynamic conditions. Palm et al. [122] developed a coupled mooring analysis technique using CFD simulations that integrated a VOF–RANS solver with Moody software, a library utilizing the local discontinuous Galerkin (LDG) method to model flexible cables without bending and torsional stiffness.

The experimental measurements of a cylindrical buoy in regular waves, moored with three slack catenary mooring cables, indicated that the surge response was solely governed by the interaction between the moorings and the body. Cevasco et al. [123] compared lumped-mass and quasistatic approaches to predict mooring line tension and fatigue in FOWTs. They concluded that while the quasistatic model yielded higher average tension values at the fairlead, the dynamic model resulted in significantly greater cumulative damage. Burmester et al. [124] coupled the quasistatic mooring model with Maritime Research Institute Netherlands' in-house time-domain solver, aNySIMxmf, and utilized the integrated model to simulate surge decay, thereby elucidating the influence of wave radiation. Jiang et al. [125] integrated a RANS solver with quasistatic and dynamic mooring models. They subsequently examined the hydrodynamic behavior of a moored buoy under regular and irregular wave conditions using various mooring models, finding that only predictions from the dynamic model consistently matched the experimental results. Chen et al. [126] developed a library named foamMooring, which integrates multiple external open-source mooring libraries with the rigid body motion solver of OpenFOAM. The primary aim is to create a CFD model coupled with several mooring analysis codes to simulate the dynamic responses of moored floating structures. Fig. 7 [126] demonstrates how the new library merges the functionalities of three mooring codes into the two rigid-body motion solvers within the OpenFOAM toolbox.

5.2. Viscous-potential flow coupling

Nevertheless, fully viscous simulations of offshore floating structures in open domains are computationally expensive. Therefore, developing viscous-potential flow coupling models is crucial for accurately predicting the hydrodynamic performance of offshore floating structures at a manageable computational cost. Potential flow effectively models wave–structure interactions but ignores viscosity and turbulence, whereas viscous flow captures localized effects such as drag and vortex shedding but requires significant computational resources. By coupling these approaches, a balance between efficiency and accuracy is achieved, enabling the simulation of critical phenomena like wave breaking, slamming, green water, flow separation, and large-amplitude motion responses in extreme sea conditions. Viscous effects are substantial and must be considered.

Numerous studies have explored the coupling of viscous and potential flow models in marine hydrodynamics. Based on the decomposition method, these coupling models can be classified into domain decomposition and functional decomposition methods. In functional decomposition coupling, the Navier–Stokes equations are locally divided into potential and viscous components, integrating the potential component within the Navier–Stokes framework. Solutions from potential flow theory are then employed to resolve the Navier–Stokes equations [127–130]. A prevalent decomposition technique is the Helmholtz decomposition, which splits the velocity field into rotational and irrotational components [131]. Building on this, the spectral wave explicit Navier–Stokes equations (SWENSE) method was developed [132]. SWENSE partitions the overall flow field into incident and complementary fields, with the entire field governed by the Navier–Stokes equations. The incident field, representing incident wave characteristics, is modeled using the Euler equations, while the complementary field is governed by the SWENSE, obtained by subtracting the Euler equations from the Navier–Stokes equations. The SWENSE method has been progressively advanced and validated for wave–structure interaction studies [133–135]. A key advantage of SWENSE is its ability to generate incident wave information on a relatively coarse mesh in the far field through explicit treatment, thereby reducing computational costs by minimizing the required grid points for wave propagation [133]. Although SWENSE effectively handles wave nonlinearity by incorporating fully nonlinear potential flows, such as the higher-order spectral (HOS) method [136], it may face difficulties with strongly nonlinear phenomena like wave breaking or extreme wave–structure interactions, where viscous and turbulent effects are significant.

Domain decomposition coupling maintains the governing equations unchanged, facilitating interaction between two methods via a coupling interface or overlapping region within their respective computational domains. A prevalent approach combines a potential flow model in the outer region with a full Navier–Stokes solver and integrates a level-set or VOF method in the inner region to simulate wave–structure interaction problems [137–139]. A coupling strategy is established between the two solvers, generally classified as one-way or two-way. The one-way coupling strategy transfers information unidirectionally, wherein the solution from one solver is passed to the other without reciprocal influence, eliminating the need for iteration between viscous and potential solvers. This strategy efficiently models wave–structure interactions during extreme wave events. For instance, coupling HOS with CFD involves nonlinear wave groups modulating over extended time and spatial scales to capture extreme wave events in random times and areas. The resulting wave fields are then extracted from the specified time range and region and applied to the wave maker of the viscous CFD solver. This one-way coupling approach is utilized by the FoamStar [133] and naoe-FOAM-SJTU solvers [140]. Conversely, the two-way coupling strategy facilitates bidirectional information exchange between the viscous and potential solvers. The computational domain and grid points were reduced. Zhong et al. [141] developed a two-way coupling strategy that integrates two open-source software packages, the finite difference method (FDM) OceanWave3D and the finite volume method (FVM) OpenFOAM, by leveraging ghost points in OceanWave3D and the

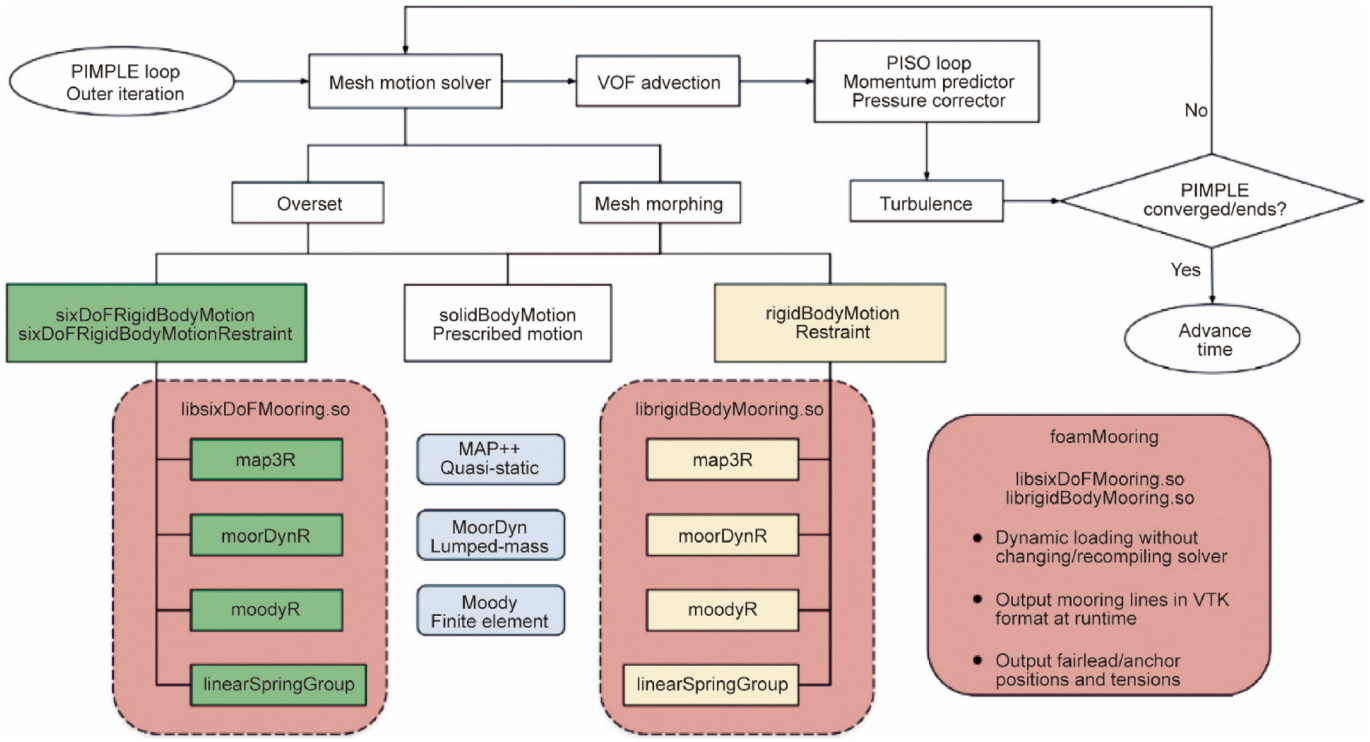

Fig. 7. Framework of the foamMooring library [126]. PIMPLE refers to the merged pressure-implicit with splitting of operators (PISO) and semi-implicit method for pressure-linked equations (SIMPLE) algorithm. MAP++, MoorDyn, and Moody are three open-source mooring analysis libraries. VTK: visualization toolkit. Reproduced from Ref. [126] with permission of Elsevier, ©2024.

relaxation zone in OpenFOAM, as illustrated in Fig. 8 [141]. Robust coupling was achieved using the fourth-order Runge–Kutta algorithm. They evaluated both 2D and 3D flows, including linear, nonlinear, irregular, and multidirectional irregular waves, demonstrating the coupling procedure's effectiveness in bidirectional data transfer. The model was validated as both accurate and efficient, offering a competitive alternative for ocean wave simulations.

5.3. Fluid–structure coupling

Large-scale floating structures frequently incorporate flexible components such as drilling risers, wind turbine towers, and blades, which experience vibrations under environmental loads. Moreover, hull structures may undergo dynamic deformation when subjected to extreme slamming loads. Accurately assessing structural integrity and performance under such conditions requires accounting for interactions between fluids and flexible or deformable structures. These fluid–structure interaction challenges can be addressed through various coupling methods, depending on the desired complexity and accuracy.

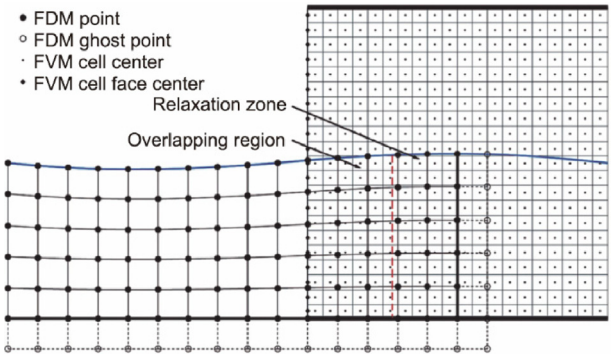

Fig. 8. Sketch of the overlapped grid system in the two-way coupling model. Reproduced from Ref. [141] with permission of Springer Nature, ©2022.

Structural dynamics are typically modeled using finite element analysis (FEA). Structural modeling may be simplified to one-dimensional (1D) representations, such as rods or beams for long, flexible components, or detailed 3D finite element meshes, based on the necessary complexity and precision. A 1D model is often employed to simulate vibrations in slender, flexible structures by reducing them to 1D elements, thereby significantly reducing computational complexity. This method is particularly advantageous when fluid forces impact large-scale structures and detailed local stress distributions are non-essential. These 1D elements primarily capture axial tension and bending moments. Fluid–structure interactions are typically calculated using quasistatic approximations or basic hydrodynamic models that apply loads (e.g., drag and lift) directly to simplified structural components. For minor deformations, Euler–Bernoulli beam theory is commonly employed to simulate flexible elements such as risers [68] and turbine blades [142]. In cases of significant deformations, nonlinear beam theory [143] or geometrically exact beam theory [144,145] is utilized to accurately represent complex nonlinear behaviors.

Alternatively, a 3D CFD–FEA model can be used, where the structure is modeled with high-fidelity finite element meshes to capture local stresses, deformations, and dynamic responses. This approach typically uses one- or two-way partitioned coupling strategies. In one-way coupling, fluid loads are transferred to the FEA model, and structural responses are calculated based on the load time history. While computationally efficient, this method ignores the added mass effect from structural elasticity, potentially missing high-frequency dynamic vibrations such as slamming-induced whipping responses [146]. Conversely, two-way coupling

considers the impact of structural deformation on the fluid domain, offering more accurate predictions of motion and wave loads [147–149].

However, two-way coupling requires greater computational resources due to the need for iterative exchanges between the CFD and FEA solvers. Prior studies have shown that two-way coupling simulations require approximately three to four times the computation time of one-way coupling simulations [146]. Nevertheless, when structural flexibility significantly affects high-frequency responses, two-way coupling provides more accurate predictions compared to experimental data [147].

5.4. Aero–hydro–mooring–aeroelastic dynamics coupling

For FOWTs, the interplay among aerodynamics, hydrodynamics, mooring dynamics, and aeroelasticity is essential to overall performance and must be comprehensively analyzed during the design phase. This necessitates developing a complex coupling model that incorporates all these effects. To explore the interactions between the rotor and wake of FOWTs, Rodriguez and Jaworski [150] integrated the free-vortex wake method into an aeroelastic numerical framework, establishing robust two-way communication between the fluid and structural domains. Owing to the lack of aeroelastic experimental data for FOWTs, validation was performed separately, focusing on aerodynamic performance and structural deformations based on experimental data. Subsequently, the validated framework was used to examine rotor–wake interactions and related aeroelastic behaviors of FOWTs under various operational scenarios [151]. Although the free-vortex wake method effectively predicts wind turbine aerodynamics under complex conditions, it does not accurately capture flow separation on blade surfaces due to the omission of fluid viscosity. Therefore, further validation is required to apply this method to FOWT aerodynamics, especially in more complex aeroelastic simulations. Consequently, a high-fidelity CFD tool is necessary for analyzing the aerohydroelastic behavior of FOWTs.

Liu et al. [143] investigated the aeroelastic characteristics of an FOWT undergoing prescribed surge motion by integrating a high-fidelity CFD solver tailored for FOWT aero-hydrodynamics with the structural solver MBDyn. In this study, blade structural deformations were computed using MBDyn based on forces on the turbine blades predicted by the fluid solver pimpleDyMFoam. The resulting deformed blade shapes were then fed back to the fluid solver, which updated the computational mesh accordingly. Their simulations not only revealed the detrimental effects of blade deformations on aerodynamic performance but also explored the impact of platform surge motion on the dynamics of flexible turbine blades. The results indicated that rotor thrust and power fluctuations increased with the application of surge motion to the platform. Subsequently, they developed a fully integrated aero–hydro–elastic tool for analyzing FOWTs under combined wind and wave conditions [152]. The effectiveness of the tool was demonstrated through the dynamic responses of a semi-submersible FOWT, including blade deformation, aerodynamic performance, platform motion, and mooring cable tension. To reduce the computational costs associated with blade-resolved CFD simulations, Huang et al. [153,154] created an aero-hydro-elastic framework for FOWTs by incorporating an actuator line model into the in-house CFD code naoe-FOAM-SJTU. The model was adapted to account for induced velocities from platform movements and blade deformations, as shown in Fig. 9 [154]. In the figure, F_L, F_D, and F_R are the lift, drag, and total force, respectively. F_N and F_T are the axial and tangential force, respectively. M_θ is the torque. The relative velocity U_{rel} is determined by the combined effects of the inflow wind speed U_{in}, blade rotation speed U_B, floating body motion-induced velocity U_M, and blade deformation-induced velocity U_S. n is the total blade element number, i is the index of blade element. δ_x, δ_y, and δ_θ are deformation along flap-wise, edge-wise, and torsional direction, respectively. Blade structures were represented using a beam model and discretized via a 1D finite element method (1D FEM). The proposed framework was validated against existing published results. They then examined the dynamic responses of a standalone FOWT and two tandem FOWTs incorporating blade deformation. The findings indicated that blade deformations led to reductions in time-averaged rotor power and thrust values, while increasing the amplitudes of their fluctuations. Additionally, the downstream FOWT experienced less blade deformation compared to the upstream unit, and more stable vortex structures were observed in the presence of blade deformations.

6. Applications

6.1. Wave breaking

Wave breaking and air–water mixed flows are critical phenomena with profound implications in coastal and ocean engineering, as they dominate the mass, energy, and momentum exchanges across the air–water interface. Cui et al. [155] conducted numerical simulations of the interaction between plunging breakers and pile groups using the open-source software REEF3D. The model was validated by comparing the predicted wave forces and FS elevations against experimental data. Peng and Chow [156] conducted numerical simulations of wave breaking over a fixed bar, comparing various wave parameters and proposing a modified version of Goda's method to analyze the reflection coefficient. Kamath et al. [157] simulated wave-breaking interactions with a vertical cylinder under five different wave height conditions. Their model accurately depicts the breaking wave process and serves as a valuable tool for assessing breaking wave forces on structures. Gu et al. [158] developed a 3D, interface-preserving level-set method to simulate dam-break flow. A dispersion-relation-preserving and compact-reconstruction weighted essentially non-oscillatory (DRP-CRWENO4) scheme was developed to achieve high-order accuracy with minimal dispersion errors in smooth regions while transitioning to compact candidate stencils to reduce oscillations near discontinuities. Wang et al. [44] employed the CLSVOF method to simulate steep Stokes wave breaking, accurately reproducing features such as the steep wave crest, overturning jet, wave plunging, air entrainment, and splash-up processes, which closely aligned with other simulation results.

Liu et al. [159] conducted comparative studies on various 2D wave-breaking scenarios and found that GFMs effectively eliminate spurious air velocities and produce wave-breaking locations consistent with experimental observations. They also compared turbulence models, concluding that the FS k–ω SST model provides the most accurate predictions of breaking waves (Fig. 10 [159]). Ferro et al. [160] implemented the GFM in OpenFOAM and validated it against typical problems, including dam breaks and periodic wave propagation. Bhushan et al. [161] compared grid resolution, turbulence models, and VOF versus CLSVOF interface models in predicting forward and backward plunging breaking waves. Both VOF and CLSVOF methods accurately capture large-scale plunging phenomena but differ in resolving finer details. The CLSVOF method outperformed in predicting secondary features such as splash-up events and secondary plungers, whereas the VOF solver provided a more precise representation of the primary plunger shape, particularly during solitary wave run-up on a slope. This highlights the strengths and limitations of each method in modeling specific aspects of complex fluid–structure interactions.

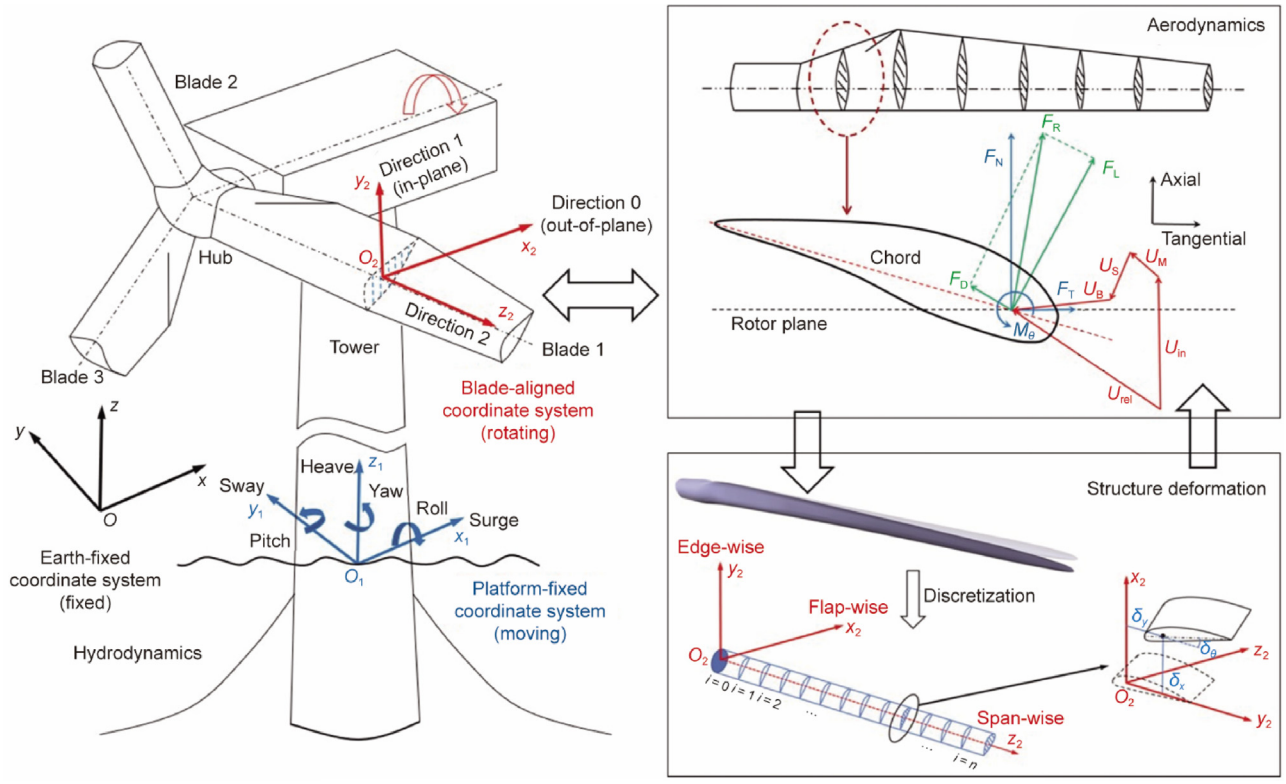

Fig. 9. Schematic diagram of the modified ALM [154].

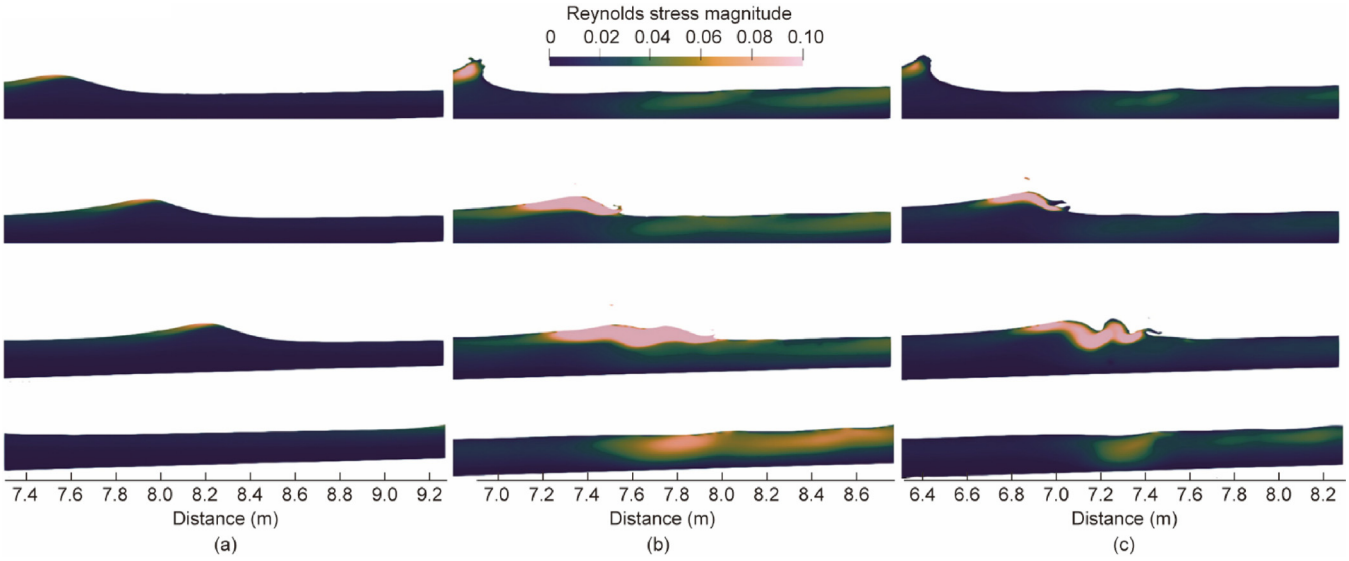

Fig. 10. The Reynolds stress magnitude contour at four different time snapshots obtained by the (a) original, (b) buoyancy modified (BM), and (c) FS k–ω SST model. Reproduced from Ref. [159] with permission of Elsevier, ©2020.

6.2. Sloshing

The importance of sloshing in FS flows is clear from its significant impact on the dynamic stability of liquid storage containers and transport vehicles. Liquid sloshing is crucial for various applications, including floating production storage and offloading (FPSO) units and liquefied natural gas (LNG) cargo vessels. Sloshing can cause highly localized impact loads, potentially resulting in severe structural damage to tank walls and ceilings. Moreover, substantial sloshing-induced forces and moments can markedly alter the motions of floating objects, which are essential for the safety and stability of offshore structures during delivery and offloading operations.

Researchers have employed various numerical methods to accurately predict liquid-sloshing phenomena. These approaches include the VOF method [162–165], level-set method [166–169], CLSVOF method [170,171], GFM [172], among others. Xin et al. [173] developed a 3D gradient-augmented level set (GALS) two-phase flow model with a pretreated reinitialization procedure to simulate violent sloshing in a cuboidal tank. Additionally, an

identification-correction technique was introduced to handle distorted FS shapes and tiny droplets, showing good agreement between the FS and pressure with experimental data. Yu et al. [169] incorporated a mass correction into the level-set method and applied it to liquid sloshing simulations. The effectiveness and accuracy of the proposed method were validated through comparative experimental results, demonstrating that the mass correction technique significantly enhances liquid sloshing stability and the precision of FS tracking. Liu et al. [171] employed the VOF and CLSVOF methods alongside four turbulence modeling strategies—the laminar flow assumption, RANS k–ε model, LES, and very LES (VLES)—to simulate sloshing flows in a rectangular tank. They found that turbulence modeling is crucial in violent sloshing simulations, whereas FS tracking plays a secondary role in nonviolent scenarios. Cai et al. [172] introduced an extended GFM for modeling liquid sloshing in incompressible multifluid systems comprising both inviscid and viscous regions. Several numerical experiments confirmed the high resolution and non-oscillatory properties of the scheme.

6.3. Slamming

A slamming event involves a sudden, brief force exerted when a body strikes a fluid or when a fluid impacts a body at a shallow angle [174]. The contact region between the fluid and the solid expands more rapidly than the impact velocity, requiring increased precision. Using the VOF method, Huang et al. [175] conducted a motion analysis of ships under various sea conditions. They identified significant bow slamming and green water occurrences in crossing seas. In symmetric cross waves, the bow flare slamming pressure along the baseline can be substantial. Asymmetric slamming impacts occur when a ship navigates an asymmetric cross-wave field. Jiao et al. [176] combined CFD with FEA, accounting for hydroelasticity, and proposed a simplified method to estimate bow flare and bottom slamming pressures based on seakeeping data of incident waves and ship global motions. Xiao et al. [149] developed a two-way coupled structure interaction approach to predict slamming loads and structural responses on a stiffened wedge, accurately capturing the peak impact pressure on the surface of the elastic structure.

Maintaining a sharp interface during numerical simulations is essential for accurately forecasting slamming loads. Xin et al. [177] developed a sharp interface multiphase flow model using a Cartesian grid solver to simulate water impact on various wedges by integrating the GALS method with the GFM. They demonstrated that the proposed sharp interface method (SIM) could accurately predict peak pressures. In the diffuse interface method (DIM), peak pressure for a small deadrise angle β_0 is underestimated by approximately 40%, as displayed in Fig. 11 [177].

Recent research highlights aeration and compressibility as critical factors in slamming loads. Elhimer et al. [178] introduced a two-phase model where an air–water mixture is treated as a homogeneous fluid with a specific equation of state, considering both water and air phases as compressible media. Gatin et al. [179,180] expanded the GFM to include a two-phase flow model with a compressible gas phase, applying it to naval hydrodynamic problems and demonstrating accurate capturing of trapped air cushioning effects.

6.4. Free-surface flow around structures

Understanding the hydrodynamic behavior of flows around stationary surface-piercing structures is essential for offshore floating structures. While single-phase flows around infinitely long submerged cylinders are well characterized, few studies have investigated the combined effects of surface piercing and free ends. Wang et al. [181] developed a sharp-interface LES methodology based on orthogonal curvilinear coordinates to simulate wave-breaking phenomena at high Reynolds numbers caused by interface-piercing bodies. They employed a level-set-based GFM for sharp interface treatment, coupled with a volume-of-fluid approach in orthogonal curvilinear coordinates to enhance interface tracking. This methodology was thoroughly validated through various numerical evaluations, including single-phase turbulent channel flow, rising air bubbles, and liquid droplet impact, demonstrating its efficacy in capturing complex two-phase flow interactions such as spray dispersion and bubble entrainment. Benitz et al. [182] conducted CFD simulations on surface-piercing cylinders with free ends and varying aspect ratios. They demonstrated that both the presence of an FS and truncated cylinder ends significantly affect hydrodynamic loads in terms of magnitude and frequency. These alterations in loading behavior are aspect ratio-dependent: At smaller penetration depths, drag is markedly reduced, and the periodic loading from vortex shedding diminishes. Chen et al. [183] modeled the flow around a vertical, surface-piercing finite circular cylinder using the geometric VOF method with the PLIC scheme. They observed pronounced 3D effects, including variations in velocity profiles, vorticity, and turbulent kinetic energy at different locations, as shown in Fig. 12 [183]. The simulations yielded comprehensive insights into the development of FS, pressure, and vorticity distributions, effectively complementing experimental results to enhance understanding of the complex wave–structure interactions.

6.5. Vortex-induced motions

The VIMs of floating offshore platforms are critical for assessing fatigue failure in mooring systems and risers. CFD has been employed to examine the VIM response characteristics of various platform types, including spars, semi-submersibles, and tension-leg platforms. Lefevre et al. [184] established and validated a set of guidelines for simulating the VIM of spar platforms using CFD. They demonstrated the ability of CFD to replicate full-scale Reynolds numbers, wave effects, mooring systems, and ocean currents by comparing CFD outcomes with high-quality scaled model test data. The study found that CFD simulations utilizing the improved delayed detached eddy simulation (IDDES) turbulence model matched model test data within a 9% margin when predicting the transverse motion of spars. Hu et al. [185] employed the IDDES model to numerically assess the VIMs of a deep-draft semi-submersible with four columns under varying current incidence angles. Through sensitivity analyses that ensured computational convergence and comparisons with experimental data, the study validated the numerical model's precision. The key conclusion was that the IDDES model reliably forecasts the VIM responses of semi-submersible platforms. Additionally, increased amplitudes in transverse motion lead to higher average drag force coefficients, which are critical considerations in the design of mooring and riser systems.

Kim et al. [186] performed experimental two-tank measurements alongside numerical simulations to investigate the VIM of a deep-draft paired-column semi-submersible (PC-Semi) platform, concentrating on cross-flow motion across different headings and reduced velocities. They successfully replicated the experimental VIM observations and confirmed the accuracy of the SST-DDES formulation. Zhao et al. [187] conducted numerical simulations on the VIMs and vortex-induced yaw (VIY) of a semi-submersible platform under two distinct current headings (0° and 45°) using the VIM-FOAM-SJTU solver and the SST-DDES turbulence model. The primary findings of the study reveal that transverse motion responses are significantly greater at 45° compared to 0°, particularly within the "lock-in" range where the vortex shedding

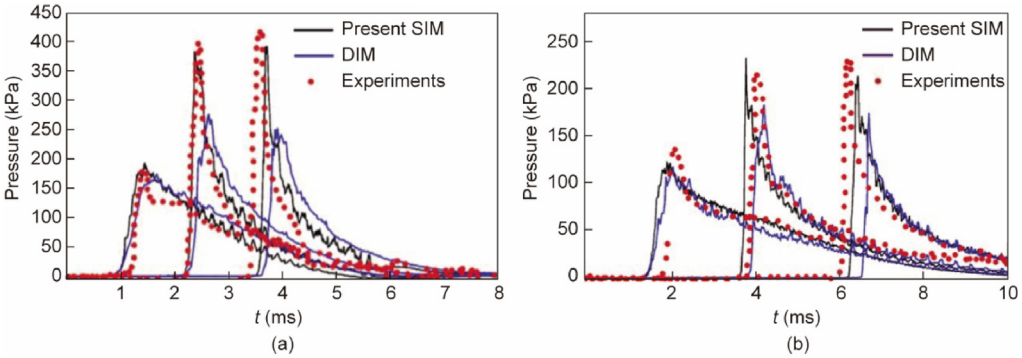

Fig. 11. Time histories of impact pressure by sharp interface and DIM. (a) β_0 = 5°, (b) β_0 = 10°. Reproduced from Ref. [177] with permission of Elsevier, ©2022.

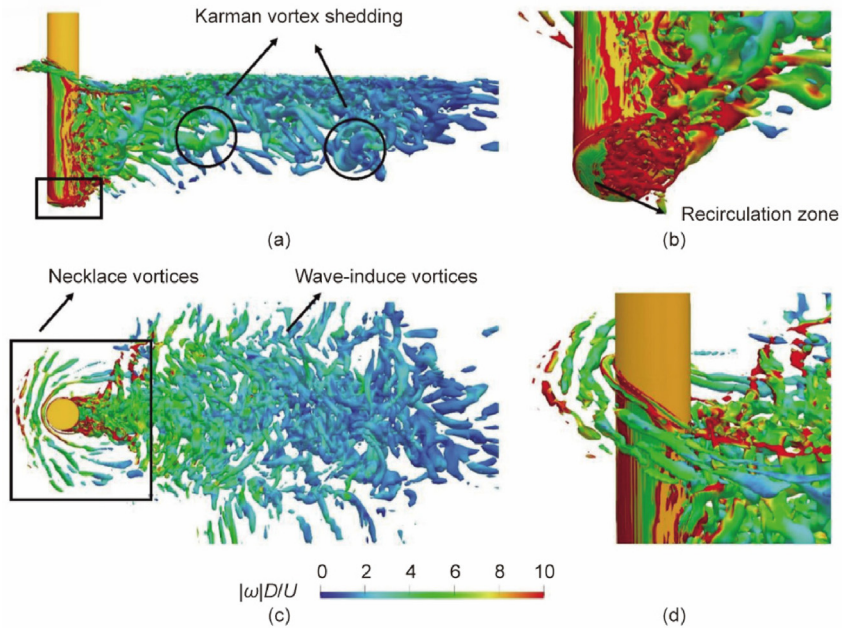

Fig. 12. Instantaneous vortical structures around a cylinder from different perspectives, colored by the nondimensionalized vorticity $|\omega|D/U$, where ω is the vorticity, D is the cylinder diameter, and U is the free stream velocity. Reproduced from Ref. [183] with permission of AIP Publishing, ©2022.

frequency synchronizes with the platform's natural frequency. Yaw motion is more prominent at 0° and is closely linked to the yaw natural period; however, the "lock-in" phenomenon was not observed in this case. Additionally, the study investigated various vortex shedding patterns and their effects on the forces and moments exerted on the platform.

6.6. Vortex-induced vibrations

Multimodal vibrations in flexible risers have been extensively explored through numerical simulations due to the complexity of riser dynamics in marine environments. CFD simulations have become indispensable for understanding the interactions between different modes and their impact on structural integrity, as well as for predicting fatigue life under continuous VIV loading. Huang et al. [64] introduced a 2D multistrip model for numerically simulating the VIV of long flexible cylinders in the time domain. The RANS method was utilized for modeling flow motion, while structural dynamics were addressed using the FEM. Initially validated under stepped flow conditions, the model successfully captured both standing and traveling wave responses of the riser, providing a comprehensive understanding of the VIV phenomenon through modal analysis, hydrodynamic force distribution, added mass coefficient, and vortex-shedding patterns. Furthermore, the model was applied to simulate shear flow conditions and demonstrated strong predictive capabilities when compared to experimental results. Duanmu et al. [65] investigated the impact of current velocity profiles, top tension, and mass ratio on flexible risers using the viv-FOAM-SJTU solver to clarify the nonlinear behavior of riser VIV, particularly under step currents. Both standing and traveling wave responses were documented across various reduced velocities. Jia et al. [188] conducted numerical simulations with a strip model to assess the VIV of deep-sea flexible risers across different aspect ratios and flow velocities. They identified and evaluated the nonlinear dynamic characteristics of flexible riser vibrations, including multifrequency, wide-frequency, and multimodal oscillations.

Beyond predicting riser VIV, several studies have explored VIV mitigation strategies employing CFD methods. Hu et al. [69,189] examined the VIV responses of flexible risers with and without top tension using the viv3D-FOAM-SJTU solver. The riser surfaces were either grooved or equipped with spanwise strips (Fig. 13 [69]). Their results demonstrated that grooves or strips can alter boundary layer separation and the wake region, thereby modifying total drag and cross-flow vibration frequencies. Proper placement of spanwise grooves and strips effectively suppresses VIV.

6.7. Moored floating platforms

By incorporating dynamic effects into the motion equations of mooring lines, dynamic analysis models provide more accurate predictions of mooring loads and, consequently, the responses of floating structures. These models surpass static and quasistatic models by capturing time-dependent factors that significantly influence the system behavior under various environmental conditions. Chen et al. [190] developed a finite-difference dynamic mooring model that incorporates cable–seabed interaction, bending stiffness, and current effects, and investigated the impact of nonlinear mooring dynamics on a spar-type FOWT subjected to current flow. Their study revealed that current loading on the mooring cables significantly affects the mooring system tension and the motion responses of the FOWT. Lee et al. [191] created a two-way coupled solver that links platform motions with the mooring system using two open-source libraries: MoorDyn and OpenFOAM. Numerical simulations for the coupled analysis of a moored floating buoy under various wave conditions demonstrated the effectiveness of the coupling in achieving more accurate predictions of hydrodynamic behavior. Huang et al. [192] integrated the finite element simulation program Mooring3D into a CFD code to simulate the 6DOF responses of a moored buoy, with results highlighting the coupled approach's advantages in addressing viscous, turbulent, and nonlinear hydrodynamic effects. Long et al. [193] incorporated a finite-element mooring model into an overset grid solver in OpenFOAM. They found that the coupled model effectively handles nonlinear resonant motions arising from interactions between irregular sea conditions and the moored floating structure, thereby demonstrating precise dynamic responses and enhanced survivability of moored floating structures under severe sea conditions.

6.8. Floating offshore wind turbines

In the context of FOWTs, the interplay among aerodynamic, hydrodynamic, and mooring dynamics is crucial. Several coupled analyses utilizing CFD simulations have been performed. Quallen and Xing [120] employed the two-phase CFD solver CFDShip-Iowa v4.5 with an overset grid technique to simulate a 5 MW FOWT. Their simulations demonstrated that generator speed fluctuations were influenced by the unsteady streamwise motions of the platform. Enhanced mooring forces in the model kept the turbine within a more favorable variable-speed control range. Consequently, the platform exhibited lower overall velocity magnitudes and reduced rotor torque, resulting in decreased rotor rotational speeds and diminished power output. Huang et al. [194] conducted numerical analyses on the coupled aero-hydrodynamic behavior of a spar-type 5 MW FOWT system. By integrating an unsteady ALM (UALM) with the two-phase CFD solver naoe-FOAM-SJTU, they solved the 3D RANS equations to investigate the intricate interactions between wind turbine aerodynamics and floating platform hydrodynamics. The UALM accounts for the dynamic motion responses of the floating platform by incorporating a velocity vector into the velocity triangle, significantly impacting the rotor wake and aerodynamic forces. This approach facilitates simulations of varying complexities to examine the coupled responses of the FOWT, revealing the substantial influence of aerodynamic forces on platform motion and the highly unsteady nature of the aerodynamic performance of the turbine owing to platform movements. Additionally, the wake vortex structures are well resolved, as depicted in Fig. 14 [194].

Zhao et al. [195] introduced a numerical model for the aerodynamic analysis of a two-bladed vertical-axis wind turbine, employing a coupled RANS approach and an ALM within the OpenFOAM library. Incorporating the k–ω SST turbulence model, the model was validated against experimental data from an H-type wind turbine, showing satisfactory agreement in thrust coefficients. The analysis uncovered significant 3D flow structures that enhance wake recovery behind the vertical-axis wind turbine, offering valuable insights for future research on closely packed contra-rotating vertical-axis turbines. The developed model is computationally efficient and lays the groundwork for predicting the dynamic response of practical vertical-axis turbines under unsteady flow conditions.

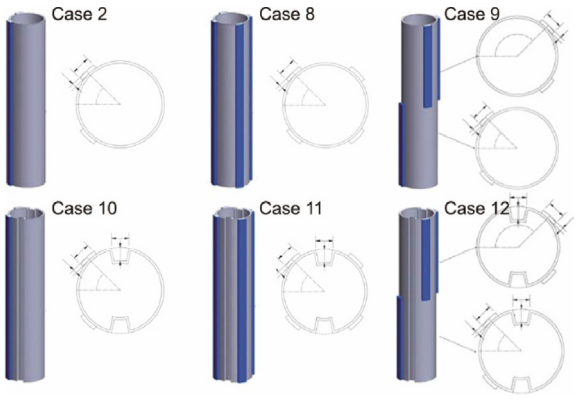

Fig. 13. Schematic diagram of 3D geometric model and 2D cross section of the grooved and/or stripped riser. Reproduced from Ref. [69] with permission of AIP Publishing, ©2022.

7. Future perspectives

CFD modeling for offshore floating structures is poised for transformative advances driven by emerging technologies and advancing computational capabilities. However, prohibitive computational costs remain a significant barrier to the widespread adoption of CFD in structural design processes. Striking an optimal balance between efficiency and accuracy is a central research challenge in this area. Several key research directions are expected to propel future progress and shape the evolution of the field.

7.1. Reduce computational cost

A primary challenge in CFD modeling is the high computational expense associated with resolving complex fluid–structure interactions and multiscale phenomena. Future research will focus on hybrid modeling approaches, such as coupling mesh-based methods (e.g., finite volume) with meshless particle methods to balance accuracy and efficiency. Graphics processing unit (GPU)-accelerated solvers will further boost computational performance [196], enabling high-fidelity simulations of large-scale offshore systems. Reduced-order models (ROMs) and surrogate modeling techniques are essential for reducing simulation times while maintaining critical accuracy, particularly in real-time applications such as operational decision-making and digital twins [197].

7.2. Integration of artificial intelligence with CFD

Integrating artificial intelligence (AI) with CFD offers a promising avenue for offshore engineering. Machine learning algorithms can develop data-driven turbulence models, optimize mesh generation, and accelerate convergence in iterative solvers. Physics-informed neural networks provide a viable alternative for directly solving PDEs, thereby eliminating conventional discretization methods while inherently preserving fundamental physical constraints. Furthermore, AI-driven surrogate models can predict

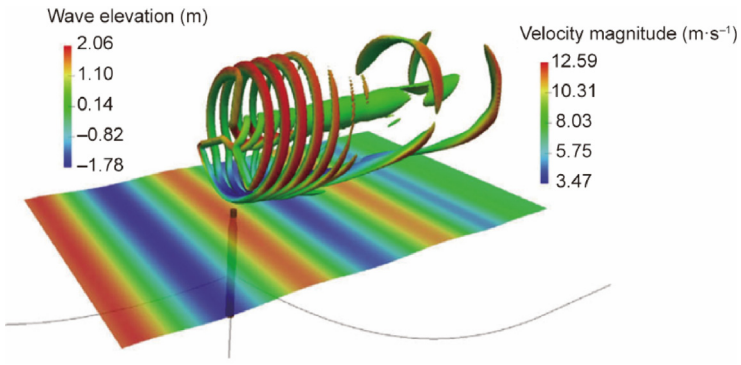

Fig. 14. Instantaneous vortex structure of the FOWT. Reproduced from Ref. [194] with permission of Springer Nature, ©2019.

hydrodynamic loads and platform responses with minimal computational overhead, facilitating rapid design exploration and uncertainty quantification.

7.3. Multiphysics and multiscale modeling

Offshore floating structures operate in complex environments involving interactions among waves, wind, currents, and structural components. Future research should focus on multiphysics coupling to accurately capture phenomena such as aero-hydroelasticity, mooring dynamics, and fluid–structure interactions. Additionally, multiscale modeling techniques bridge macroscale wave dynamics and microscale turbulence, enabling comprehensive simulations of offshore systems under extreme conditions.

7.4. High-performance computing and exascale simulations

The advent of exascale computing will revolutionize CFD capabilities, allowing unprecedented resolution and accuracy in simulating offshore floating structures. Utilizing high-performance computing (HPC) frameworks enables researchers to perform large-scale, high-fidelity simulations of entire offshore platforms, including detailed modeling of mooring lines, risers, and floating wind turbines. Consequently, the development of novel design concepts and operational strategies will ensure safer and more efficient offshore systems.

7.5. Validation and uncertainty quantification

As CFD models become increasingly sophisticated, the necessity for stringent validation and uncertainty quantification intensifies. To guarantee reliability in engineering applications, forthcoming research must integrate experimental data and field measurements with numerical simulations. This approach aims to bolster CFD model accuracy and dependability by contrasting simulations with actual performance data. Benchmarking scenarios, such as those for FOWTs proposed by the International Energy Agency, are crucial for validation. These standardized conditions enable the testing and refinement of CFD predictions, offering insights into numerical model performance within dynamic offshore settings.

8. Closing remarks

This study provides a comprehensive overview of the current and future capabilities of CFD in designing and analyzing offshore floating structures. By synthesizing cutting-edge methodologies and applications, this study underscores the unmatched capacity of CFD to address intricate multiphysics phenomena, including nonlinear wave–structure interactions, turbulent wake dynamics, and fluid–structure coupling. These phenomena are vital for ensuring structural integrity, operational safety, and performance efficiency in harsh marine environments. Key advancements in two-phase interfacial flow modeling, turbulence closure schemes tailored for wave and wake flows, and robust coupling algorithms for multicomponent systems and multibody dynamics are critically examined, demonstrating their transformative impact on predicting hydrodynamic loads, motion responses, and the structural integrity of offshore platforms.

With computational power advancing to exascale levels, CFD is set to revolutionize offshore engineering by optimizing green technologies like floating wind turbines and enhancing the resilience of deep-water oil and gas infrastructures. By reducing numerical diffusion, lowering computational costs, and overcoming user proficiency barriers, CFD will become indispensable for navigating the complexities of ocean environments. This advancement will ultimately enhance safety, efficiency, and sustainability in offshore development. This review synthesizes past achievements and presents a roadmap for future research, underscoring the pivotal role of CFD as a foundation for innovation in marine and offshore engineering.

CRediT authorship contribution statement

Weiwen Zhao: Writing – original draft, Visualization, Validation, Methodology, Investigation, Formal analysis, Data curation. **Wentao Wang:** Writing – original draft, Investigation, Formal analysis, Data curation. **Genglu Zhang:** Visualization, Validation, Methodology, Investigation. **Decheng Wan:** Writing – review & editing, Validation, Supervision, Software, Resources, Project administration, Funding acquisition, Conceptualization. **Frederick Stern:** Writing – review & editing, Investigation, Data curation. **Moustafa Abdel-Maksoud:** Writing – review & editing, Validation, Data curation.

Declaration of competing interest

The authors declare that they have no known competing financial interests or personal relationships that could have appeared to influence the work reported in this paper.

Acknowledgments

This work was supported by the National Natural Science Foundation of China (52131102) and the Research and Application Demonstration Project of Key Technologies for Safeguarding Container Vessels in Ningbo Zhoushan Port Based on Intelligent Navigation (ZJHG-FW-2024-27), for which the authors are grateful.

References

[1] Nematbakhsh A, Bachynski EE, Gao Z, Moan T. Comparison of wave load effects on a TLP wind turbine by using computational fluid dynamics and potential flow theory approaches. Appl Ocean Res 2015;53:142–54.
[2] Sulovsky I, de Hauteclocque G, Greco M, Prpić-Oršić J. Comparative study of potential flow and CFD in the assessment of seakeeping and added resistance of ships. J Mar Sci Eng 2023;11(3):641.
[3] Babanin A, Bernardino M, Von Bock Und Polach F, Campos R, Ding J, Van Essen S, et al. Report of committee I.1: environment. In: Proceedings of the 21st international ship and offshore structures congress, 2022 Sep 11–15, Vancouver, BC, Canada. Alexandria: SNAME; 2022.
[4] Hermundstad OA, Chai S, De Hauteclocque G, Dong S, Fang CC, Johannessen TB, et al. Report of Committee I.2: loads. In: Proceedings of the 21st international ship and offshore structures congress, 2022 Sep 11–15, Vancouver, BC, Canada. Alexandria: SNAME; 2022.
[5] Tavakoli S, Khojasteh D, Haghani M, Hirdaris S. A review on the progress and research directions of ocean engineering. Ocean Eng 2023;272:113617.
[6] Temarel P, Bai W, Bruns A, Derbanne Q, Dessi D, Dhavalikar S, et al. Prediction of wave-induced loads on ships: progress and challenges. Ocean Eng 2016;119:274–308.
[7] Wang J, Wan D. Application progress of computational fluid dynamic techniques for complex viscous flows in ship and ocean engineering. J Mar Sci Appl 2020;19(1):1–16.
[8] Zhang W, Calderon-Sanchez J, Duque D, Souto-Iglesias A. Computational fluid dynamics (CFD) applications in floating offshore wind turbine (FOWT) dynamics: a review. Appl Ocean Res 2024;150:104075.
[9] Mirjalili S, Ivey CB, Mani A. Comparison between the diffuse interface and volume of fluid methods for simulating two-phase flows. Int J Multiph Flow 2019;116:221–38.
[10] Ubbink O, Issa RI. A method for capturing sharp fluid interfaces on arbitrary meshes. J Comput Phys 1999;153(1):26–50.
[11] Muzaferija S. Peric M, Sames PC, Schellin TE. A two-fluid Navier–Stokes solver to simulate water entry. In: Proceeding of the 22nd symposium of naval hydrodynamics, 1998 Aug 9–14, Washington, DC, USA. Washington, DC: National Academies Press; 1999, p. 638–51.
[12] Darwish M, Moukalled F. Convective schemes for capturing interfaces of free-surface flows on unstructured grids. Numer Heat Transf B 2006; 49(1):19–42.
[13] Heyns JA, Malan AG, Harms TM, Oxtoby OF. Development of a compressive surface capturing formulation for modelling free-surface flow by using the volume-of-fluid approach. Int J Numer Methods Fluids 2013;71(6):788–804.
[14] Zhang D, Jiang C, Liang D, Chen Z, Yang Y, Shi Y. A refined volume-of-fluid algorithm for capturing sharp fluid interfaces on arbitrary meshes. J Comput Phys 2014;274:709–36.
[15] Rusche H. Computational fluid dynamics of dispersed two-phase flows at high phase fractions [dissertation]. London: Imperial College London; 2002.
[16] Larsen BE, Fuhrman DR, Roenby J. Performance of interFoam on the simulation of progressive waves. Coast Eng J 2019;61(3):380–400.
[17] Xiao F, Honma Y, Kono T. A simple algebraic interface capturing scheme using hyperbolic tangent function. Int J Numer Methods Fluids 2005;48 (9):1023–40.
[18] Yokoi K. Efficient implementation of THINC scheme: a simple and practical smoothed VOF algorithm. J Comput Phys 2007;226(2):1985–2002.
[19] Xiao F, Ii S, Chen C. Revisit to the THINC scheme: a simple algebraic VOF algorithm. J Comput Phys 2011;230(19):7086–92.
[20] Cifani P, Michalek WR, Priems GJM, Kuerten JGM, van der Geld CWM, Geurts BJ. A comparison between the surface compression method and an interface reconstruction method for the VOF approach. Comput Fluids 2016;136:421–35.
[21] Noh WF, Woodward P. SLIC (simple line interface calculation). In: Vooren AI, Zandbergen PJ, editors. Proceedings of the Fifth international conference on numerical methods in fluid dynamics, 1976 Jun 28–Jul 2, Enschede, The Netherlands. Berlin: Springer Nature; 1976. p. 330–40.
[22] Youngs DL. Time-dependent multi-material flow with large fluid distortion. In: Numerical methods for fluid dynamics. New York City: Academic Press; 1982. p. 273–85.
[23] Roenby J, Bredmose H, Jasak H. A computational method for sharp interface advection. R Soc Open Sci 2016;3(11):160405.
[24] Scheufler H, Roenby J. Accurate and efficient surface reconstruction from volume fraction data on general meshes. J Comput Phys 2019;383:1–23.
[25] Cummins SJ, Francois MM, Kothe DB. Estimating curvature from volume fractions. Comput Struc 2005;83(6–7):425–34.
[26] Esteban A, López J, Gómez P, Zanzi C, Roenby J, Hernández J. A comparative study of two open-source state-of-the-art geometric VOF methods. Comput Fluids 2023;250:105725.
[27] Scheufler H, Roenby J. TwoPhaseFlow: a framework for developing two phase flow solvers in OpenFOAM. OpenFOAM® J 2023;3:200–24.
[28] Dai D, Tong AY. Analytical interface reconstruction algorithms in the PLIC–VOF method for 3D polyhedral unstructured meshes. Int J Numer Methods Fluids 2019;91(5):213–27.
[29] López J, Hernández J. gVOF: an open-source package for unsplit geometric volume of fluid methods on arbitrary grids. Comput Phys Commun 2022;277:108400.
[30] Osher S, Sethian JA. Fronts propagating with curvature-dependent speed: algorithms based on Hamilton–Jacobi formulations. J Comput Phys 1988;79 (1):12–49.
[31] Sethian JA, Smereka P. Level set methods for fluid interfaces. Annu Rev Fluid Mech 2003;35(1):341–72.
[32] du Chéné A, Min C, Gibou F. Second-order accurate computation of curvatures in a level set framework using novel high-order reinitialization schemes. J Sci Comput 2008;35(2–3):114–31.
[33] Enright D, Fedkiw R, Ferziger J, Mitchell I. A hybrid particle level set method for improved interface capturing. J Comput Phys 2002;183(1):83–116.
[34] Herrmann M. A balanced force refined level set grid method for two-phase flows on unstructured flow solver grids. J Comput Phys 2008;227 (4):2674–706.
[35] Gibou F, Fedkiw R, Osher S. A review of level-set methods and some recent applications. J Comput Phys 2018;353:82–109.
[36] Olsson E, Kreiss G. A conservative level set method for two phase flow. J Comput Phys 2005;210(1):225–46.
[37] Olsson E, Kreiss G, Zahedi S. A conservative level set method for two phase flow II. J Comput Phys 2007;225(1):785–807.
[38] Chiodi R, Desjardins O. A reformulation of the conservative level set reinitialization equation for accurate and robust simulation of complex multiphase flows. J Comput Phys 2017;343:186–200.
[39] Shervani-Tabar N, Vasilyev OV. Stabilized conservative level set method. J Comput Phys 2018;375:1033–44.
[40] Bahbah C, Khalloufi M, Larcher A, Mesri Y, Coupez T, Valette R, et al. Conservative and adaptive level-set method for the simulation of two-fluid flows. Comput Fluids 2019;191:104223.
[41] Sussman M, Puckett EG. A coupled level set and volume-of-fluid method for computing 3D and axisymmetric incompressible two-phase flows. J Comput Phys 2000;162(2):301–37.
[42] Kunkelmann C, Stephan P. Modification and extension of a standard volume-of-fluid solver for simulating boiling heat transfer. In: Pereira JCF, Sequeira A, editors. Proceedings of the 5th European conference on computational fluid dynamics ECCOMAS CFD2010, 2010 Jun 14–17, Lisbon, Portugal. Barcelona: CIMNE Congress Bureau; 2010.
[43] Albadawi A, Donoghue DB, Robinson AJ, Murray DB, Delauré YMC. Influence of surface tension implementation in volume of fluid and coupled volume of fluid with level set methods for bubble growth and detachment. Int J Multiph Flow 2013;53:11–28.
[44] Wang Z, Yang J, Koo B, Stern F. A coupled level set and volume-of-fluid method for sharp interface simulation of plunging breaking waves. Int J Multiph Flow 2009;35(3):227–46.
[45] Dianat M, Skarysz M, Garmory A. A coupled level set and volume of fluid method for automotive exterior water management applications. Int J Multiph Flow 2017;91:19–38.
[46] Skarysz M, Garmory A, Dianat M. An iterative interface reconstruction method for PLIC in general convex grids as part of a coupled level set volume of fluid solver. J Comput Phys 2018;368:254–76.
[47] Zhao Y, Chen HC. A new coupled level set and volume-of-fluid method to capture free surface on an overset grid system. Int J Multiph Flow 2017;90:144–55.
[48] Afshar MA. Numerical wave generation in OpenFOAM® [dissertation]. Goeteborg: Chalmers University of Technology; 2010.
[49] Fedkiw RP, Aslam T, Merriman B, Osher S. A non-oscillatory Eulerian approach to interfaces in multimaterial flows (the ghost fluid method). J Comput Phys 1999;152(2):457–92.
[50] Kang M, Fedkiw RP, Liu XD. A boundary condition capturing method for multiphase incompressible flow. J Sci Comput 2000;15(3):323–60.
[51] Huang J, Carrica PM, Stern F. Coupled ghost fluid/two-phase level set method for curvilinear body-fitted grids. Int J Numer Methods Fluids 2007;55 (9):867–97.
[52] Yang J, Stern F. Sharp interface immersed-boundary/level-set method for wave–body interactions. J Comput Phys 2009;228(17):6590–616.
[53] Wang Z, Stern F. Volume-of-fluid based two-phase flow methods on structured multiblock and overset grids. Int J Numer Methods Fluids 2022;94(6):557–82.
[54] Vukčević V, Jasak H, Gatin I. Implementation of the ghost fluid method for free surface flows in polyhedral finite volume framework. Comput Fluids 2017;153:1–19.
[55] Peltonen P, Kanninen P, Laurila E, Vuorinen V. The ghost fluid method for OpenFOAM: a comparative study in marine context. Ocean Eng 2020;216:108007.
[56] Peltonen P, Kanninen P, Laurila E, Vuorinen V. Scaling effects on the free surface backward facing step flow. Phys Fluids 2021;33(4):042106.
[57] Kanninen P, Peltonen P, Vuorinen V. Full-scale ship stern wave with the modelled and resolved turbulence including the hull roughness effect. Ocean Eng 2022;245:110434.
[58] Chen S, Zhao W, Wan D. On the scattering of focused wave by a finite surface-piercing circular cylinder: a numerical investigation. Phys Fluids 2022;34 (3):035132.
[59] Kamath A, Fleit G, Bihs H. Investigation of free surface turbulence damping in RANS simulations for complex free surface flows. Water 2019;11(3):456.
[60] Devolder B, Troch P, Rauwoens P. Performance of a buoyancy-modified k–ω and k–ω SST turbulence model for simulating wave breaking under regular waves using OpenFOAM®. Coast Eng 2018;138:49–65.

[61] Larsen BE, Fuhrman DR. On the over-production of turbulence beneath surface waves in Reynolds-averaged Navier–Stokes models. J Fluid Mech 2018;853:419–60.
[62] Willden RHJ, Graham JMR. Numerical prediction of VIV on long flexible circular cylinders. J Fluids Struct 2001;15(3–4):659–69.
[63] Willden RHJ, Graham JMR. Multi-modal vortex-induced vibrations of a vertical riser pipe subject to a uniform current profile. Eur J Mech B/Fluids 2004;23(1):209–18.
[64] Huang Z, Deng Z, Liu D, Bai Y. Numerical simulation for VIV of a long flexible cylinder in the time domain. Ships Offshore Struct 2018;13(Supp1):214–27.
[65] Duanmu Y, Zou L, Wan D. Numerical analysis of multi-modal vibrations of a vertical riser in step currents. Ocean Eng 2018;152:428–42.
[66] Fu B, Wan D. Numerical study of vibrations of a vertical tension riser excited at the top end. J Ocean Eng Sci 2017;2(4):268–78.
[67] Fu B, Zou L, Wan D. Numerical study of vortex-induced vibrations of a flexible cylinder in an oscillatory flow. J Fluids Struct 2018;77:170–81.
[68] Deng D, Zhao W, Wan D. Vortex-induced vibration prediction of a flexible cylinder by three-dimensional strip model. Ocean Eng 2020;205:107318.
[69] Hu H, Zhao W, Wan D. Vortex-induced vibration of a slender flexible riser with grooved and spanwise strips subject to uniform currents. Phys Fluids 2022;34(12):125131.
[70] Yin D, Passano E, Jiang F, Lie H, Wu J, Ye N, et al. State-of-the-art review of vortex-induced motions of floating offshore wind turbine structures. J Mar Sci Eng 2022;10(8):1021.
[71] Spalart PR. Detached-eddy simulation. Annu Rev Fluid Mech 2009;41(1):181–202.
[72] Kim SJ, Spernjak D, Holmes S, Vinayan V, Antony A. Vortex-induced motion of floating structures: CFD sensitivity considerations of turbulence model and mesh refinement. In: Proceedings of the 34th international conference on ocean, offshore and arctic engineering; 2015 May 31–Jun 5, St. John's, NL, Canada. New York City: American Society of Mechanical Engineers (ASME); 2015. p. V002T08A057.
[73] Kara M, Kaufmann J, Gordon R, Sharma P, Lu J. Application of CFD for computing VIM of floating structures. In: Proceedings of the offshore technology conference, 2016 May 2–5, Houston, Texas, USA. London: Onepetro; 2016. p. OTC-26950-MS.
[74] Chen CR, Chen HC. Simulation of vortex-induced motions of a deep draft semi-submersible in current. Ocean Eng 2016;118:107–16.
[75] Sørensen JN, Shen WZ. Numerical modeling of wind turbine wakes. J Fluids Eng 2002;124(2):393–9.
[76] Bachant P, Goude A, Wosnik M. Actuator line modeling of vertical-axis turbines. arXiv: 1605.01449; 2016.
[77] Stevens RJAM, Martínez-Tossas LA, Meneveau C. Comparison of wind farm large eddy simulations using actuator disk and actuator line models with wind tunnel experiments. Renew Energy 2018;116:470–8.
[78] Carrica PM, Wilson RV, Noack RW, Stern F. Ship motions using single-phase level set with dynamic overset grids. Comput Fluids 2007;36(9):1415–33.
[79] Shen Z, Wan D. RANS computations of added resistance and motions of a ship in head waves. Int J Offshore Polar Eng 2013;23:263–71.
[80] Shen Z, Wan D, Carrica PM. Dynamic overset grids in OpenFOAM with application to KCS self-propulsion and maneuvering. Ocean Eng 2015;108:287–306.
[81] Dullweber A, Leimkuhler B, McLachlan R. Symplectic splitting methods for rigid body molecular dynamics. J Chem Phys 1997;107(15):5840–51.
[82] Dunbar AJ, Craven BA, Paterson EG. Development and validation of a tightly coupled CFD/6-DOF solver for simulating floating offshore wind turbine platforms. Ocean Eng 2015;110(Pt A):98–105.
[83] Chow JH, Ng EYK. Strongly coupled partitioned six degree-of-freedom rigid body motion solver with Aitken's dynamic under-relaxation. Int J Nav Archit Ocean Eng 2016;8(4):320–9.
[84] Bruinsma N, Paulsen BT, Jacobsen NG. Validation and application of a fully nonlinear numerical wave tank for simulating floating offshore wind turbines. Ocean Eng 2018;147:647–58.
[85] Devolder B, Troch P, Rauwoens P. Accelerated numerical simulations of a heaving floating body by coupling a motion solver with a two-phase fluid solver. Comput Math Appl 2019;77(6):1605–25.
[86] Roenby J, Aliyar S, Bredmose H. A robust algorithm for computational floating body dynamics. R Soc Open Sci 2024;11(4):231453.
[87] Jasak H, Tuković Ž. Dynamic mesh handling in OpenFOAM applied to fluid–structure interaction simulations. In: Proceedings of the fifth European conference on computational fluid dynamics ECCOMAS CFD 2010, 2010 Jun 14–17, Lisbon, Portugal. Barcelona: CIMNE Congress Bureau; 2010.
[88] Chen H, Hall M. CFD simulation of floating body motion with mooring dynamics: coupling MoorDyn with OpenFOAM. Appl Ocean Res 2022;124:103210.
[89] Helenbrook BT. Mesh deformation using the biharmonic operator. Int J Numer Methods Eng 2003;56(7):1007–21.
[90] Batina JT. Unsteady Euler airfoil solutions using unstructured dynamic meshes. AIAA J 1990;28(8):1381–8.
[91] Yang Z, Mavriplis D. Unstructured dynamic meshes with higher-order time integration schemes for the unsteady Navier–Stokes equations. In: Proceedings of the 43rd AIAA aerospace sciences meeting and exhibit, 2005 Jan 10–13, Reno, NV, USA. Reston: American Institute of Aeronautics and Astronautics (AIAA); 2005. p. 1–13.
[92] Shamsaei B, Newman JC. Comparison of linear and non-linear elasticity large displacement mesh deformation in computational fluid dynamics. In: Proceedings of the 46th AIAA fluid dynamics conference, 2016 Jun 13–17, Washington, DC, USA. Reston: American Institute of Aeronautics and Astronautics (AIAA); 2016. p. 3183.
[93] Estruch O, Lehmkuhl O, Borrell R, Pérez Segarra CD, Oliva A. A parallel radial basis function interpolation method for unstructured dynamic meshes. Comput Fluids 2013;80:44–54.
[94] Li CN, Wei Q, Gong CL, Gu LX. An efficient multiple point selection study for mesh deformation using radial basis functions. Aerosp Sci Technol 2017;71:580–91.
[95] Tang X, Luo J, Liu F. Adjoint aerodynamic optimization of a transonic fan rotor blade with a localized two-level mesh deformation method. Aerosp Sci Technol 2018;72:267–77.
[96] Witteveen J. Explicit and robust inverse distance weighting mesh deformation for CFD. In: Proceedings of the 48th AIAA aerospace sciences meeting including the new horizons forum and aerospace exposition, 2010 Jan 4–7, Orlando, FL, USA. Reston: American Institute of Aeronautics and Astronautics (AIAA); 2010. p. 1–10.
[97] Tran TT, Kim DH. Fully coupled aero-hydrodynamic analysis of a semi-submersible FOWT using a dynamic fluid body interaction approach. Renew Energy 2016;92:244–61.
[98] Chandar DDJ. On overset interpolation strategies and conservation on unstructured grids in OpenFOAM. Comput Phys Commun 2019;239:72–83.
[99] Teschner F, Mundt Ch. Fully conservative overset mesh to overcome the blunt body metric singularity in finite difference methods. Shock Waves 2022;32(3):295–312.
[100] Quon EW, Smith MJ. Advanced data transfer strategies for overset computational methods. Comput Fluids 2015;117:88–102.
[101] Rinaldi E, Colonna P, Pecnik R. Flux-conserving treatment of non-conformal interfaces for finite-volume discretization of conservation laws. Comput Fluids 2015;120:126–39.
[102] Griffith BE, Patankar NA. Immersed methods for fluid–structure interaction. Annu Rev Fluid Mech 2020;52(1):421–48.
[103] Kim W, Choi H. Immersed boundary methods for fluid–structure interaction: a review. Int J Heat Fluid Flow 2019;75:301–9.
[104] Verzicco R. Immersed boundary methods: historical perspective and future outlook. Annu Rev Fluid Mech 2023;55(1):129–55.
[105] Peskin CS. Flow patterns around heart valves: a numerical method. J Comput Phys 1972;10(2):252–71.
[106] Goldstein D, Handler R, Sirovich L. Modeling a no-slip flow boundary with an external force field. J Comput Phys 1993;105(2):354–66.
[107] Saiki EM, Biringen S. Numerical simulation of a cylinder in uniform flow: application of a virtual boundary method. J Comput Phys 1996;123(2):450–65.
[108] Mohd-Yosuf J. Combined immersed-boundary/B-spline methods for simulations of flow in complex geometries. Annu Res Briefs 1997;1997:317–27.
[109] Majumdar S, Iaccarino G, Durbin P. RANS solvers with adaptive structured boundary non-conforming grids. Annu Res Briefs 2001;2001:353–66.
[110] Tseng YH, Ferziger JH. A ghost-cell immersed boundary method for flow in complex geometry. J Comput Phys 2003;192(2):593–623.
[111] Souza PRC, Neto HR, Villar MM, Vedovotto JM, Cavalini Jr AA, Neto AS. Multi-phase fluid–structure interaction using adaptive mesh refinement and immersed boundary method. J Braz Soc Mech Sci Eng 2022;44(4):152.
[112] Borthwick A, Cruz León S, Jozsa J. Adaptive quadtree model of shallow-flow hydrodynamics. J Hydraul Res 2001;39(4):413–24.
[113] Popinet S. An accurate adaptive solver for surface-tension-driven interfacial flows. J Comput Phys 2009;228(16):5838–66.
[114] Popinet S. Gerris: a tree-based adaptive solver for the incompressible Euler equations in complex geometries. J Comput Phys 2003;190(2):572–600.
[115] Fuster D, Bagué A, Boeck T, Le Moyne L, Leboissetier A, Popinet S, et al. Simulation of primary atomization with an octree adaptive mesh refinement and VOF method. Int J Multiph Flow 2009;35(6):550–65.
[116] Sui Y, Spelt PD. Validation and modification of asymptotic analysis of slow and rapid droplet spreading by numerical simulation. J Fluid Mech 2013;715:283–313.
[117] Gunney BTN, Anderson RW. Advances in patch-based adaptive mesh refinement scalability. J Parallel Distrib Comput 2016;89:65–84.
[118] Liu Y, Peng Y, Wan D. Numerical investigation on interaction between a semi-submersible platform and its mooring system. In: Proceedings of the ASME 2015 34th international conference on ocean, offshore and arctic engineering, 2015 May 31–Jun 05, St. John's, NL, Canada. New York City: American Society of Mechanical Engineers (ASME); 2015. p. V007T06A071.
[119] Smith RJ, MacFarlane CJ. Statics of a three component mooring line. Ocean Eng 2001;28(7):899–914.
[120] Quallen S, Xing T. CFD simulation of a floating offshore wind turbine system using a variable-speed generator-torque controller. Renew Energy 2016;97:230–42.
[121] Gutiérrez-Romero JE, García-Espinosa J, Serván-Camas B, Zamora-Parra B. Non-linear dynamic analysis of the response of moored floating structures. Mar Struct 2016;49:116–37.
[122] Palm J, Eskilsson C, Paredes GM, Bergdahl L. Coupled mooring analysis for floating wave energy converters using CFD: formulation and validation. Int J Mar Energy 2016;16:83–99.
[123] Cevasco D, Collu M, Rizzo C, Hall M. On mooring line tension and fatigue prediction for offshore vertical axis wind turbines: a comparison of lumped mass and quasi-static approaches. Wind Eng 2018;42(2):97–107.

[124] Burmester S, Vaz G, Gueydon S, el Moctar O. Investigation of a semi-submersible floating wind turbine in surge decay using CFD. Ship Technol Res 2020;67(1):2–14.
[125] Jiang C, el Moctar O, Schellin TE, Paredes GM. Comparative study of mathematical models for mooring systems coupled with CFD. Ships Offshore Struct 2021;16(9):942–54.
[126] Chen H, Medina TA, Cercos-Pita JL. CFD simulation of multiple moored floating structures using OpenFOAM: an open-access mooring restraints library. Ocean Eng 2024;303:117697.
[127] Ducrozet G, Engsig-Karup AP, Bingham HB, Ferrant P. A non-linear wave decomposition model for efficient wave–structure interaction. Part A: formulation, validations and analysis. J Comput Phys 2014;257:863–83.
[128] Vukčević V, Jasak H, Malenica Š. Decomposition model for naval hydrodynamic applications, part II: verification and validation. Ocean Eng 2016;121:76–88.
[129] Li Z. Two-phase spectral wave explicit Navier–Stokes equations method for wave–structure interactions [dissertation]. Nantes: École centrale de Nantes; 2018.
[130] Yu J, Yao C, Liu L, Dong G, Zhang Z. Numerical study on wave–structure interaction based on functional decomposition method. Ocean Eng 2022;266:113067.
[131] Dommermuth DG. The laminar interactions of a pair of vortex tubes with a free surface. J Fluid Mech 1993;246:91–115.
[132] Ferrant P, Gentaz L, Le Touze D. A new RANSE/potential approach for water wave diffraction. In: Proceedings of the 5th numerical towing tank. Symposium 2002 (NuTTS'02), 2002 Sep 29–Oct 2, Pornichet, France. Red Hook: Curran Associates Inc.; 2002. p. 1–6.
[133] Aliyar S, Ducrozet G, Bouscasse B, Sriram V, Ferrant P. Efficiency and accuracy of the domain and functional decomposition strategies for the wave–structure interaction problem. Ocean Eng 2022;266:112568.
[134] Lao T, Li Z, Wang Z, Wang Z, Yang Z. Generation of incident wave in two-phase flow simulation based on field decomposition. Ocean Eng 2023;285:115256.
[135] Shen C, Chen NZ. A SWENSE-based wave-induced loading simulation for a semi-submersible FOWT platform. Ocean Eng 2024;311:118950.
[136] Ducrozet G, Bonnefoy F, Le Touzé D, Ferrant P. A modified high-order spectral method for wavemaker modeling in a numerical wave tank. Eur J Mech BFluids 2012;34:19–34.
[137] Colicchio G, Greco M, Faltinsen OM. A BEM-level set domain-decomposition strategy for non-linear and fragmented interfacial flows. Int J Numer Methods Eng 2006;67(10):1385–419.
[138] Paulsen BT, Bredmose H, Bingham HB. An efficient domain decomposition strategy for wave loads on surface piercing circular cylinders. Coast Eng 2014;86:57–76.
[139] Zhuang Y, Wan D. Parametric study of a new HOS–CFD coupling method. J Hydrodynam 2021;33(1):43–54.
[140] Zhuang Y, Zhao W, Wan D. The nonlinearity of scattering waves due to interaction between focusing waves and floating production storage and offloading. Phys Fluids 2023;35(10):107113.
[141] Zhong W, Wang W, Wan D. Coupling potential and viscous flow models with domain decomposition for wave propagations. J Hydrodynam 2022;34 (5):826–48.
[142] Zheng J, Wang N, Wan D, Strijhak S. Numerical investigations of coupled aeroelastic performance of wind turbines by elastic actuator line model. Appl Energy 2023;330:120361.
[143] Liu Y, Xiao Q, Incecik A, Peyrard C. Aeroelastic analysis of a floating offshore wind turbine in platform-induced surge motion using a fully coupled CFD–MBD method. Wind Energy 2019;22(1):1–20.
[144] Wang Q, Sprague MA, Jonkman J, Johnson N, Jonkman B. BeamDyn: a high-fidelity wind turbine blade solver in the FAST modular framework. Wind Energy 2017;20(8):143962.
[145] Wu X, Feng K, Li Q. A numerical method for the dynamics analysis of blade fracture faults in wind turbines using geometrically exact beam theory and its validation. Energies 2024;17(4):824.
[146] Benra FK, Dohmen HJ, Pei J, Schuster S, Wan B. A comparison of one-way and two-way coupling methods for numerical analysis of fluid–structure interactions. J Appl Math 2011;2011(1):853560.
[147] Lakshmynarayanana PAK, Hirdaris S. Comparison of nonlinear one- and two-way FFSI methods for the prediction of the symmetric response of a containership in waves. Ocean Eng 2020;203:107179.
[148] Takami T, Iijima K. Numerical investigation into combined global and local hydroelastic response in a large container ship based on two-way coupled CFD and FEA. J Mar Sci Technol 2020;25(2):346–62.
[149] Xiao J, Liu C, Han B, Wan D, Wang J. A two-way coupled fluid–structure interaction method for predicting the slamming loads and structural responses on a stiffened wedge. Phys Fluids 2024;36(7):077123.
[150] Rodriguez SN, Jaworski JW. Strongly-coupled aeroelastic free-vortex wake framework for floating offshore wind turbine rotors. Part 1: numerical framework. Renew Energy 2019;141:1127–45.
[151] Rodriguez SN, Jaworski JW. Strongly-coupled aeroelastic free-vortex wake framework for floating offshore wind turbine rotors. Part 2: application. Renew Energy 2020;149:1018–31.
[152] Liu Y, Xiao Q. Development of a fully coupled aero–hydro–mooring–elastic tool for floating offshore wind turbines. J Hydrodynam 2019;31(1): 21–33.
[153] Huang Y, Wan D, Hu C. Numerical analysis of aero-hydrodynamic responses of floating offshore wind turbine considering blade deformation. In: Proceedings of the 31st international ocean and polar engineering conference, 2021 Jun 20–25, Rhodes, Greece. Mountain View: International Society of Offshore and Polar Engineers (ISOPE); 2021. p. 450–8.
[154] Huang Y, Xiao Q, Wan D. Wake interaction between two floating offshore wind turbines with blade deformation. In: Proceedings of the ASME 2022 41st international conference on ocean offshore and arctic engineering, 2010 Jun 5–10, Hamburg, Germany. Washington: American Society of Mechanical Engineers (ASME); 2022. p. V008T09A014.
[155] Cui T, Kamath A, Wang W, Yuan L, Han D, Bihs H. Focused plunging breaking waves impact on pile group in finite water depth. J Offshore Mech Arctic Eng 2022;144(3):031202.
[156] Peng NN, Chow KW. A numerical wave tank with large eddy simulation for wave breaking. Ocean Eng 2022;266:112555.
[157] Kamath A, Alagan Chella M, Bihs H, Arntsen ØA. Breaking wave interaction with a vertical cylinder and the effect of breaker location. Ocean Eng 2016;128:105–15.
[158] Gu ZH, Wen HL, Yu CH, Sheu TWH. Interface-preserving level set method for simulating dam-break flows. J Comput Phys 2018;374:249–80.
[159] Liu S, Ong MC, Obhrai C, Gatin I, Vukčević V. Influences of free surface jump conditions and different k–ω SST turbulence models on breaking wave modelling. Ocean Eng 2020;217:107746.
[160] Ferro P, Landel P, Pescheux M, Guillot S. Development of a free surface flow solver using the ghost fluid method on OpenFOAM. Ocean Eng 2022;253:111236.
[161] Bhushan S, El Fajri O, Hubbard G, Chambers B, Kees C. Assessment of numerical methods for plunging breaking wave predictions. J Mar Sci Eng 2021;9(3):264.
[162] Nicolici S, Bilegan RM. Fluid structure interaction modeling of liquid sloshing phenomena in flexible tanks. Nucl Eng Des 2013;258:51–6.
[163] Tahmasebi MK, Shamsoddini R, Abolpour B. Performances of different turbulence models for simulating shallow water sloshing in rectangular tank. J Mar Sci Appl 2020;19(3):381–7.
[164] Vallés Rebollo X, Sadeghi E, Kusano I, García-Granada AA. Study of the sloshing dynamics in partially filled rectangular tanks with submerged baffles using VOF and LES turbulence methods for different impact angles. Computation 2022;10(12):225.
[165] Zhuang Y, Wang G, Wan D, Wu J. Numerical simulations of FPSO with sloshing tanks in a random freak waves. J Hydrodynam 2022;34(3):491–8.
[166] Wang C, Teng J, Huang GPG. Numerical simulation of sloshing motion inside a two dimensional rectangular tank by level set method. Int J Numer Methods Heat Fluid Flow 2011;21(1):5–31.
[167] Bai W, Liu X, Koh CG. Numerical study of violent LNG sloshing induced by realistic ship motions using level set method. Ocean Eng 2015;97:100–13.
[168] Battaglia L, Cruchaga M, Storti M, D'Elía J, Núñez Aedo J, Reinoso R. Numerical modelling of 3D sloshing experiments in rectangular tanks. Appl Math Model 2018;59:357–78.
[169] Yu J, Yue B, Ma B. Isogeometric analysis with level set method for large-amplitude liquid sloshing. Ocean Eng 2022;265:112613.
[170] Zhao Y, Chen HC. Numerical simulation of 3D sloshing flow in partially filled LNG tank using a coupled level-set and volume-of-fluid method. Ocean Eng 2015;104:10–30.
[171] Liu D, Tang W, Wang J, Xue H, Wang K. Modelling of liquid sloshing using CLSVOF method and very large eddy simulation. Ocean Eng 2017;129:160–76.
[172] Cai L, Zhou J, Zhou F, Xie W, Nie Y. Numerical simulation of 2D liquid sloshing. Int J Appl Mech 2012;04(2):1250014.
[173] Xin J, Shi F, Jin Q, Ma L. Gradient-augmented level set two-phase flow method with pretreated reinitialization for three-dimensional violent sloshing. J Fluids Eng 2019;142(1):011402.
[174] Dias F, Ghidaglia JM. Slamming: recent progress in the evaluation of impact pressures. Annu Rev Fluid Mech 2018;50(1):243–73.
[175] Huang S, Jiao J, Chen C. Numerical prediction of ship motion and slamming load characteristics in cross wave. J Mar Sci Technol 2022;27(1):104–24.
[176] Jiao J, Huang S, Tezdogan T, Terziev M, Guedes SC. Slamming and green water loads on a ship sailing in regular waves predicted by a coupled CFD–FEA approach. Ocean Eng 2021;241:110107.
[177] Xin J, Shi F, Fan S, Jin Q. A sharp interface multiphase flow model for two-dimensional water impact of a symmetric and asymmetric wedge. Appl Ocean Res 2022;119:102988.
[178] Elhimer M, Jacques N, El Malki AA, Gabillet C. The influence of aeration and compressibility on slamming loads during cone water entry. J Fluids Struct 2017;70:24–46.
[179] Gatin I, Vladimir N, Malenica Š, Jasak H. Green sea loads in irregular waves with finite volume method. Ocean Eng 2019;171:554–64.
[180] Gatin I, Liu S, Vukčević V, Jasak H. Finite volume method for general compressible naval hydrodynamics. Ocean Eng 2020;196:106773.
[181] Wang Z, Suh J, Yang J, Stern F. Sharp interface LES of breaking waves by an interface piercing body in orthogonal curvilinear coordinates. In: Proceedings of the 50th AIAA aerospace sciences meeting including the new horizons forum and aerospace exposition, 2012 Jan 9–12, Nashville, TN, USA. Reston: American Institute of Aeronautics and Astronautics (AIAA); 2012. p. 1111.
[182] Benitz MA, Carlson DW, Seyed-Aghazadeh B, Modarres-Sadeghi Y, Lackner MA, Schmidt DP. CFD simulations and experimental measurements of flow

past free-surface piercing, finite length cylinders with varying aspect ratios. Comput Fluids 2016;136:247–59.
[183] Chen S, Zhao W, Wan D. Turbulent structures and characteristics of flows past a vertical surface-piercing finite circular cylinder. Phys Fluids 2022;34 (1):015115.
[184] Lefevre C, Constantinides Y, Kim JW, Henneke M, Gordon R, Jang H, et al. Guidelines for CFD simulations of spar VIM. Proceedings of the 32nd international conference on offshore mechanics and arctic engineering, Nantes, France, 2013.
[185] Hu X, Zhang X, You Y. Numerical studies on vortex-induced motions of a semi-submersible with four columns based on IDDES model. In: Proceedings of the ASME 2017 36th international conference on ocean, offshore and arctic engineering, 2017 Jun 25–30, Trondheim, Norway. Washington: The American Society of Mechanical Engineers (ASME); 2017. p. V001T01A056.
[186] Kim SJ, Spernjak D, Mejia-Alvarez R, Vinayan V, Sterenborg J, Antony A, et al. Numerical simulation of vortex-induced motion of a deep-draft paired-column semi-submersible offshore platform. Ocean Eng 2018;149:291–304.
[187] Zhao W, Wei Z, Wan D. Numerical investigation on the effects of current headings on vortex induced motions of a semi-submersible. J Hydrodynam 2022;34(3):382–94.
[188] Jia L, Sang S, Shi X, Shen F. Investigation on numerical simulation of VIV of deep-sea flexible risers. Appl Sci 2023;13(14):8096.
[189] Hu H, Pan Z, Zhao W, Wan D. Numerical investigation of vortex-induced vibrational responses to a flexible tensioned riser with symmetric grooves in uniform currents. Ocean Eng 2023;271:113780.
[190] Chen L, Basu B, Nielsen SRK. A coupled finite difference mooring dynamics model for floating offshore wind turbine analysis. Ocean Eng 2018;162:304–15.
[191] Lee SC, Song S, Park S. Platform motions and mooring system coupled solver for a moored floating platform in a wave. Processes 2021;9(8):1393.
[192] Huang H, Gu H, Chen HC. A new method to couple FEM mooring program with CFD to simulate six-DOF responses of a moored body. Ocean Eng 2022;250:110944.
[193] Long Y, Liu Y, Zhao Z, Liu F. Coupling a nonlinear finite element mooring model with an overset CFD solver for dynamic analysis of floating structures in waves. Ocean Eng 2024;307:118183.
[194] Huang Y, Cheng P, Wan D. Numerical analysis of a floating offshore wind turbine by coupled aero-hydrodynamic simulation. J Mar Sci Appl 2019;18 (1):82–92.
[195] Zhao R, Creech ACW, Borthwick AGL, Venugopal V, Nishino T. Aerodynamic analysis of a two-bladed vertical-axis wind turbine using a coupled unsteady RANS and actuator line model. Energies 2020;13(4):776.
[196] Piscaglia F, Ghioldi F. GPU acceleration of CFD simulations in OpenFOAM. Aerospace 2023;10(9):792.
[197] Fresca S, Manzoni A. Real-time simulation of parameter-dependent fluid flows through deep learning-based reduced order models. Fluids 2021;6 (7):259.